STATE OF ALASKA
DEPARTMENT OF NATURAL RESOURCES

Alaska Geologic Materials Center

Data Report #430

Cook Inlet Energy LLC, 2015, Rock: Fluid compatibility - Regain permeability; Rock mechanics: Formation hardness of Hemlock Formation cores after immersion in water and oil based fracturing fluids; and Analysis of coreplugs and wholecore segments from the Redoubt Unit #02 well

---

Received Feb 2015

All data reports may be downloaded free of charge from the DGGS website

Advancing Reservoir Performance

T-14-12-1209SCA

Rock:Fluid Compatibility – Regain Permeability

Pressure Pumping Technology Center, Tomball

COOK INLET ENERGY
REDOUBT UNIT 02
REDOUBT SHOAL OIL FIELD
KENAI PENNINSULA BOROUGH, ALASKA

TECHNICAL REPRESENTATIVES: EDWIN POST
ANCHORAGE, AK

13 JANUARY 2015

www.bakerhughes.com

© 2011 Baker Hughes Incorporated. All rights reserved. This report may contain confidential customer information and should not be discussed, provided to or otherwise disclosed to anyone outside of Baker Hughes other than the customer or authorized customer representative.

OBJECTIVE

Results presented in this report reflect testing performed to assess compatibility between formation core and several water-based fluids. Formation core material from the subject well was received for use in this study. Reports containing petrological and geomechanical data will follow under separate cover.

Regain oil permeability presented herein is the comparison of effective permeability to oil at irreducible water saturation (KoSwi) prior to and after wellbore injected fluids. Laboratory testing was performed at 195°F.

RESULTS

Previously drilled and cleaned samples, as well as newly drilled core samples, were provided for this study. The newly drilled samples were batch extracted of hydrocarbons and residual salts with a low boiling temperature solvent. The previously drilled samples were obtained with fresh water and, as this was a study of clay reaction, were eliminated from selection. Basic properties of all core samples are presented on page 2.

Based on permeability and sample condition, two samples from 14492.30 feet were halved to provide a matched pair. Dry nitrogen permeability was NOT re-measured on the halved samples.

SUMMARY OF REGAIN OIL PERMEABILITY

Sample ID	Depth, feet	Permeability, md			Regain, percent	Fluid System
		to N_2	KoSwi			
			Initial	Final		
2A-1	14492.30	4.93	1.94	1.51	78	3% KCl + 1 gpt ClayMaster-5C
2A-2			2.45	1.93	79	SpectraStar 4000, broken/filtered
2B-1		4.81	1.77	1.90	107	3% KCl
2B-2			1.75	1.74	100	3% KCl = 1 gpt ClayMaster-10

Regain oil permeability after 3% KCl + 1 gpt ClayMaster-5C (CM-5C) and the broken/filtered SpectraStar 4000 was 78-79% of the original KoSwi. Regain oil permeability after 3% KCl only exceeded 100% of the original KoSwi, suggesting that CM-5C was potentially decreasing the regain. A test using CM-10, the replacement for CM-5C, indicated no damage from the inclusion of the product in a 3% KCl solution.

The SpectraStar 4000 and synthetic formation brine formulations are below.

SpectraStar 4000 Based in 3% KCl	Loading
GW3LDF	10 gpt
BF-8L	2 gpt
FloBack 30	1 gpt
ClayMaster-5C	1 gpt
XLW-24	2.5 gpt
Enzyme G	1 gpt
CRB	3 gpt

Synthetic Brine	
Component	gm/liter
NaCl	13.4
$CaCl_2*2H_2O$	17.6
$MgCl_2*6H_2O$	0.284
Na_2SO_4	0.998
KCl	0.172

PROCEDURES

Sample Preparation

Previously extracted 1.0" diameter core plugs and 2/3 slabbed sections from the subject well were provided for use in this study. From the slabbed sections, using Isopar-L as the bit coolant and lubricanat, 1.0" diameter core plugs were drilled. The newly drilled samples were extracted as a batch using a low boiling point solvent. All samples were dried to stable weights in a low temperature (150°F) convection oven.

Basic properties of permeability and porosity were determined. Clean and dry permeability to dry nitrogen gas was determined under minimal confining stress (250 psi) OR 1500 psi, depending upon the permeability equipment. Grain volume was determined at ambient pressure. Pore volume, porosity and grain density were calculated.

SUMMARY OF BASIC PROPERTIES

ID	Depth, ft.	Permeability to N2, md	Confining Pressure, psi	Porosity, percent	Grain Density, gm/cc	Condition
2A	14492.30	4.93	250	12.9	2.66	oil drill
2B		4.81	250	13.0	2.66	oil drill
4A	14551.00	92.7	250	13.8	2.64	oil drill
4B		72.1	250	13.5	2.65	oil drill
5	14551.30	Not suitable				water drill
6A	14801.80	1.15	250	24.4	2.63	oil drill
6B		0.0508	1500	12.3	2.63	oil drill
7A	14848.20	0.0201	1500	14.0	2.64	oil drill
7B		<0.0010	1500	15.9	2.64	oil drill
9	14924.30	61.9	250	21.4	2.64	water drill
13	15002.70	40.7	250	9.3	2.65	water drill
14	15025.70	15.7	250	9.9	2.64	water drill

Regain Permeability to Oil

The sample test was evacuated and saturated with synthetic formation brine. The saturated sample was loaded into a preheated (195°F), vertically oriented hydrostatic-load coreholder. Approximately 1500 psi net confining stress was applied and maintained throughout. All fluids were injected against 300 psi back pressure.

1. By constant rate, Isopar-L (mineral oil) was injected to establish irreducible water saturation. Differential pressure was monitored/recorded and effective permeability to oil (KoSwi) was calculated.
2. Treatments were injected at the same rate in the opposing direction in volumes as noted on the chart.
3. Return oil permeability was in the initial direction at the same rate. Differential pressure was monitored/recorded and regain KoSwi was calculated.

Test 1: 3% KCl + 1 gpt CM-5C

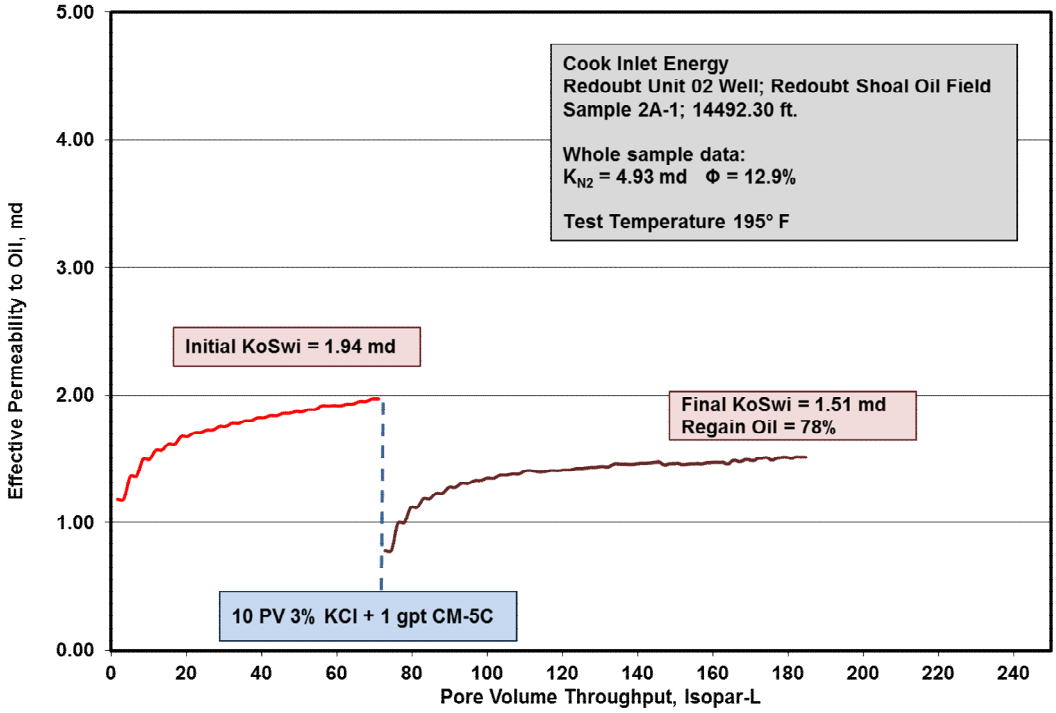

Test 2: Broken/Filtered SpectraStar 4000

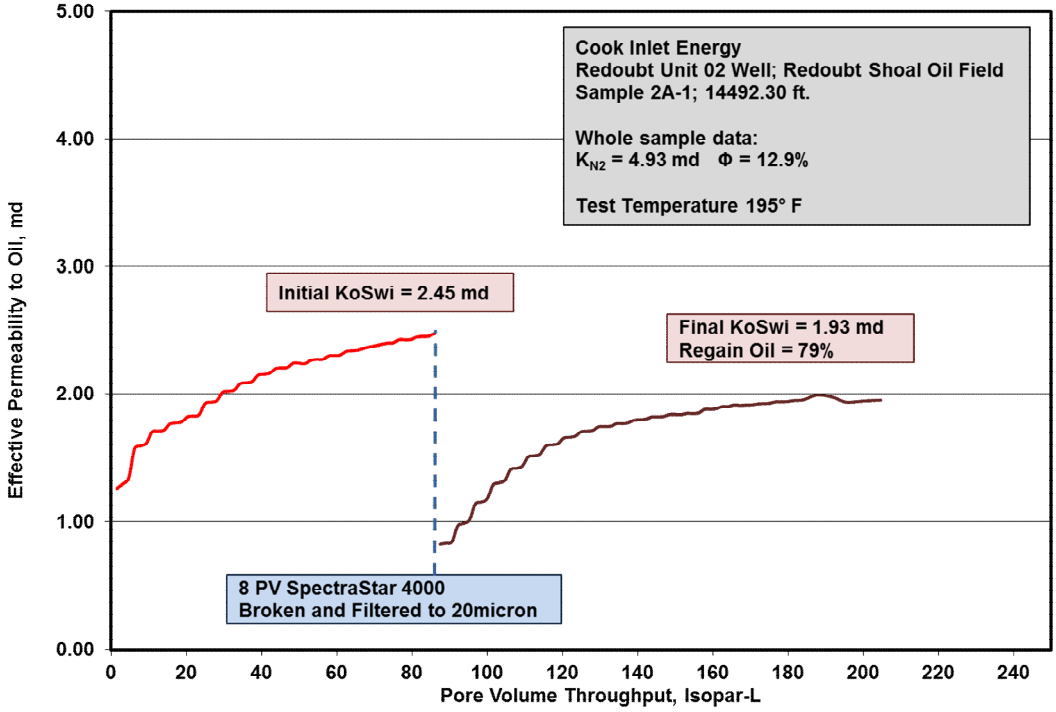

Test 3: 3% KCl only

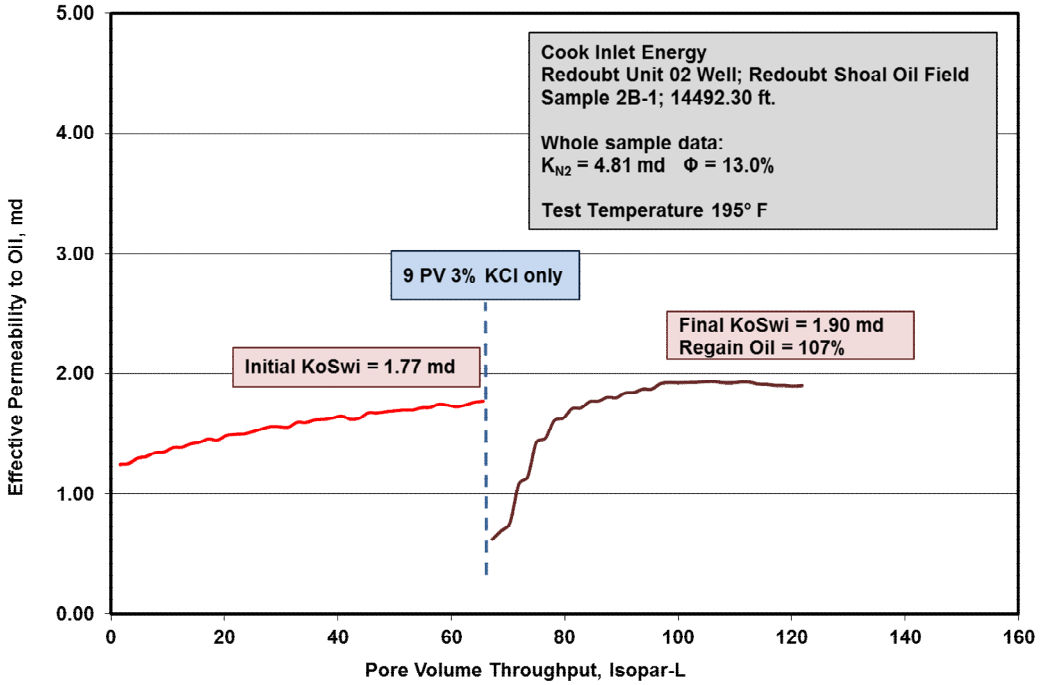

Test 4: 3% KCl + 1 gpt CM-10

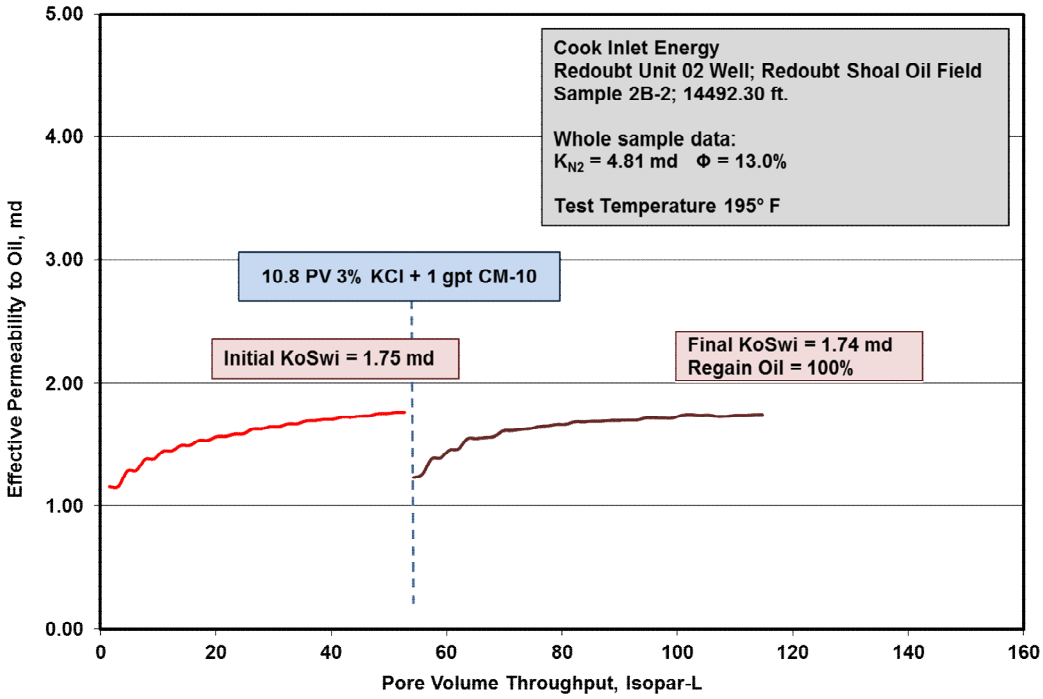

Technology Center Report No.	T-14-12-1209
Reported by:	Jennifer Cutler
Requested by:	Edwin Post
Location:	Anchorage, Alaska
Analyzed by:	Michael Cowell
Distribution:	Edwin Post, Kenneth Nix, Joshua Herald, Dave Susko
Additional Distribution:	PPTC File

The above data is supplied solely for informational purposes, and Baker Hughes makes no guarantees or warranties, either expressed or implied, with respect to the accuracy or use of these data and interpretations. All product warranties and guarantee shall be governed by the standard contract terms at the time of sale.

Advancing Reservoir Performance

BAKER HUGHES

T- 14-12-1209 Rock Mechanics

Formation Hardness of Hemlock Formation Cores after Immersion in Water and Oil Based Fracturing Fluids

Pressure Pumping Technology Center, Tomball

COOK INLET ENERGY
OFFSHORE COOK INLET, ALASKA
REDOUBT UNIT FIELD
HEMLOCK SANDSTONE/CONGLOMERATE FORMATION
REDOUBT RU-02 WELL
API# 50-733-20501-0000

TECHNICAL REPRESENTATIVE: EDWIN POST
KENAI, ALASKA

JANUARY 28, 2015

© 2011 Baker Hughes Incorporated. All rights reserved. This report may contain confidential customer information and should not be discussed, provided to or otherwise disclosed to anyone outside of Baker Hughes other than the customer or authorized customer representative.

CONTENTS

EXECUTIVE SUMMARY

Formation hardness and elastic properties of Hemlock formation cores from the Cook Inlet are reported. Reductions in formation hardness were measured on cores after immersion in tap water, synthetic oil, and 3% KCl based SpectraStar for up to five days and at 190 °F. The post-immersion Brinell hardness values were used to estimate embedment of a single layer of proppant at minimum and maximum net closure stress. Young's modulus, Poisson's Ratio, and compressive strength were measured on a sub-set of formation brine saturated cores under confining stress of 4675 psi and 72 °F.

Results showed Young's modulus varying from approximately 1x106 psi in the Upper Hemlock oil-rich sandstone to 3.2x106 psi in the cobble conglomerate of the Lower Hemlock. Poisson's Ratio varied from 0.24 to 0.42, although the higher value is suspect of bias from possible damage incurred during the initial hydrostatic ramp. Compressive strength of the cobble conglomeritic sandstone was about 3 times greater than found in the pebble and finer grained sandstone intervals.

There was no dramatic difference in the reduction of formation hardness from their initial values after immersion in either fluid. The formation hardness showed a tendency to increase from the softer well sorted sandstone in Upper Hemlock (BH = 28-35 kg/mm^2) to BH = 50-100 kg/mm^2 in the pebble conglomerate to BH = 100 – 150 kg/mm^2 in the cobble conglomerate (Lower Hemlock).

Estimated of proppant embedment, based on estimates of formation pressure and minimum horizontal stress gradients, indicated that proppant embedment is expected to be controlled the in-situ formation hardness and drawdown pressure applied to the fracture during production. At maximum net closure stress (maximum drawdown), embedment, in terms of a fraction of the proppant diameter, is expected to vary from 16%-22% in the softer oil-rich sandstone to only 3%-4% in the cobble conglomerate. For wide fractures containing multiple layers of proppant, embedment should have little adverse effect on fracture conductivity. For areas of the fracture with a single layer or less of proppant, embedment have a greater detrimental effect.

INTRODUCTION

This report contains the laboratory test results of formation hardness and elastic properties of Hemlock formation core material from the RU-02 well. This report was part of a larger effort to understand the sensitivity of the cored interval to water-based fracturing fluids. Methods employed, and previously reported, include X-ray Diffraction that tests for mineral content[1], Capillary Suction Time (CST)[1] that tests the "expandability" of clay minerals to the fluid, and regain permeability[2] that measures the loss of formation permeability after exposure to fracturing fluids.

The objective of the work, herein, was to test the sensitivity of formation hardness to water based fracturing fluids. For this purpose, the Brinell (BH) method was employed. The post-immersion BH values are useful for estimating proppant embedment as a function net closure stress, especially in soft formations hydraulically fractured with low proppant concentrations and produced at high drawdown pressures.

The fluids used in this study were tap water, SpectraStar™, and Synoil (oil-based fluid for Super RheoGel™). The tap water and oil-based fluids were used to set upper and lower bounds to the clay mineral fluid sensitivity. The freshwater is potentially the most damaging in terms of reduction in hardness, while the oil-based fluid is the least damaging. The SpectraStar tested was a 3% KCl based fracturing fluid that had been used in previous treatments and was a candidate fluid for future treatments. The cores were immersed for up to five days at reservoir temperature of 190 ^{o}F.

Young's modulus and Poisson's Ratio of a few core samples (those that were long enough for triaxial testing) were also measured. The cores were initially saturated in a brine solution prepared from reported water analysis[3] from the RU-02 well. Tests were conducted under confining stress of 4675 psi, which is approximately equal to reservoir net mean stress. These elastic constants are required input into numerical hydraulic fracture models, and the static values of these constants are often used to calibrate mechanical property logs derived from wireline density-dipole sonic measurements.

CORE DESCRIPTIONS

Whole core sections from fifteen depth intervals were shipped to PPTC for evaluation. The whole cores spanned the upper and lower Hemlock formation. Core spanned depths from14429 feet to 15026 feet. Except for cores #2 (14492.3 feet), #4 (14551.0 feet), #15 (14877.3 feet?), and #13 (15002.7 feet), all cores were described[1] as pebble conglomerates. Core #15 was a naturally fractured shale/mudstone. Oil stain was observed in cores #2, #4 and #10.

Brinell hardness was measured on a subset of the whole core sections, as listed in Table 1. Photographs of the pre-immersion core samples are located in Appendix IV.

Table 1
Core Samples Used for Immersion Testing

Formation	Core Depth (ft)	Core ID	As Received Wt. (gm)	Immersion Fluid
U. Hemlock	14492.3	2a	12.256	tap water
		2b	15.609	SpectraStar
		2c*	12.296	Synoil
		2d	8.075	Synoil
	14551.0	4a	10.509	tap water
		4b	8.876	SpectraStar
		4c*	10.356	Synoil
		4d	8.898	Synoil
L. Hemlock	14801.8	6a	17.299	Synoil
		6b	23.449	tap water
		6c	31.253	SpectraStar
		6d*	37.841	Synoil
	14848.2	7a	39.317	tap water
		7b	23.712	SpectraStar
		7c*	31.321	Synoil
		7d	13.712	Synoil
	14905.0	8	27.667	SpectraStar
	14940.0	11a	12.099	tap water
		11b	7.424	Synoil
		11d	9.091	SpectraStar
		11e*	9.778	Synoil

*these cores were contaminated with tap water early in the procedure and were replaced by companion samples (see discussion).

Table 2
Core Plugs Used for Triaxial Tests

Formation	Core Depth (ft)	Core ID	Length (in.)	Dia. (in.)	L/D Ratio	Sat. Bulk Density (g/cc)
U. Hemlock	14551.0	4a	1.462	1.01	1.45	2.427
		4b	1.667	1.01	1.65	2.429
L. Hemlock	14848.2	7	1.549	1.012	1.53	2.501
L. Hemlock	15002.7	13	1.479	0.978	1.51	2.451
L. Hemlock	14877.3?	15	1.440	0.979	1.47	Nd*

*core #15 broke apart upon immersion in the prepared formation brine.

IMMERSION FLUIDS

The synthetic formation brine was formulated using the following salts. The salt concentrations were determined from the Core Laboratories water analysis report[3] on the RU-2 well. This solution was used to saturated cores assigned to mechanical property testing.

Table 3
Synthetic Brine Composition

Synthetic Brine[2]	
Component	**gm/liter**
NaCl	13.4
$CaCl_2*2H_2O$	17.6
$MgCl_2*6H_2O$	0.284
Na_2SO_4	0.998
KCl	0.172

The SpectraStar 4000 was formulated from the following chemical ingredients. The fluid was broken and filtered prior to core immersion. The base water was 3% KCl.

Table 4
SpectraStar Composition for Immersion Tests

SpectraStar 4000 Based in 3% KCl [2]	**Loading**
GW3LDF	10 gpt
BF-8L	2 gpt
FloBack 30	1 gpt
ClayMaster-5C	1 gpt
XLW-24	2.5 gpt
Enzyme G	1 gpt
CRB	3 gpt

RESULTS & INTERPRETATIONS

Static Elastic Properties

Young's modulus and Poisson's Ratio were measured on select cores. Each core was vacuum saturated with the synthetic formation brine (Table 3). The elastic constants were measured under "drained" conditions, at room temperature (72 ^{o}F), and a confining stress of 4675 psi (i.e. reservoir net mean stress). Axial deviatoric stress was cycled twice and the elastic constants evaluated from the 2nd cycle between 0% and 50% of the peak strength. The test procedures are described in detail in Appendix I.

Reservoir net mean stress was estimated from reported and assumed reservoir stress and pressure gradients:

a. Rock overburden gradient = 1 psi/ft;
b. Seawater pressure gradient = 0.45 psi/ft;
c. Reservoir pressure gradient, G_r = 0.45 psi/ft;
d. Closure stress = 7725 psi;
e. Minimum horizontal stress gradient, G_{hmin} = 7725 psi/14780' = 0.523 psi/ft;
f. Average core depth = 14780 feet;
g. Biot-Willis poroelastic constant, α = 0.8;
h. Sea water depth = 450 feet.

Total overburden stress = Seawater pressure + subsea rock overburden pressure.

σ_o = (14780' – 450') x1 psi/ft + 450' x 0.45 psi/ft = 14530 psi (or 0.983 psi/ft).

Reservoir net mean stress, σ'_m, resulted in a value of:

$\sigma'_m = \{(G_o + 2G_{hmin})/3 - \alpha G_r\}D_{avg}$. = {(0.983 psi/ft +2x0.523 psi/ft)/3 – 0.8x0.45 psi/ft} x14780' = 4675 psi.

The results of the testing are shown in Table 5. Stress-strain curves for each test is located in Appendix II. Core photographs are located in Appendix III.

Immersion Testing

Immersion testing was undertaken to address the concern that candidate fracturing fluids may sufficiently soften the surfaces of hydraulic fractures to where excessive proppant embedment would occur. The concern was raised primarily by the friable texture and the existence of illite/smectite that was detected in some of the cored intervals. These minerals were found to contain a relatively high percentage of the expandable form of smectite and, therefore, potentially very sensitive to the salinity of the water in which they would be exposed.

Past experience has shown that the variability in hardness per location on the core surfaces often exceeds or equals the variability in hardness per fluid type (except when comparing changes in BH between initially dry and immersed states). Consequently, the more subtle changes in hardness due to water salinity are often masked by the heterogeneity of cores, themselves. Given that the core was not preserved, any reductions in hardness between the partially dry and initially fluid immersed states would not a true measure of the effects of the

fluids being tested. Therefore, in this study, each core sample was immersed in one of the three fluids for a few hours at room temperature before measuring its initial formation hardness. This BH value was used as the basis of comparison for the long term effect of immersion. Also, tap water and oil based fluids were selected to generate the extreme changes in hardness at each cored interval. If the formation is sensitive to water salinity, then there should be a clear and measurable difference in BH between the fresh water and oil immersed cores. Large differences in BH would justify testing at different KCl salinities, while small differences would preclude the need for a more detailed evaluation of different KCl concentrations.

The initial dry weights were also recorded. The weight of each core was measured after a few hours immersion and after the 4-5 day immersion. The increase in weight with immersion time is located in Appendix V.

Three to four indentation tests were performed on the core sample surfaces. The Brinell hardness was then calculated for each indentation. The average and standard deviation were calculated and recorded.

The tap water and SpectraStar immersed cores were immersed for five days in a water bath set at 190 ^{o}F. The oil immersed cores were immersed for only four days at 190 ^{o}F. The shorter immersion time was due to having to prepare a new set of core samples after tap water was discovered inside the vials containing the cores. The new set of oil-immersed samples was subsequently placed inside a glass container and immersed in the water bath.

The results of the average values and standard deviations of BH are shown in Table 6 and Figures 1 through 5. The error bars in these figures represent the standard deviations of each set of three to four measurements. Pre-immersion photographs of the core samples are located in Appendix IV.

Estimates of Proppant Embedment Tests

The average values of post-immersion BH were used to estimate the amount of embedment that could be expected in a hydraulic fracture supported by a single layer of proppant subjected to the anticipated minimum and maximum net closure stress. The results are shown in the Table 7.

The calculation was based on a simple model of a single layer of non-deformable proppant arranged in a hexagonal close-pack array pressed between the surfaces of a smooth fracture. An expression was derived for calculating the reduction in fracture width, $\Delta w_f/w_f$, as a function of BH and net closure stress and is presented in Appendix I. The end result is stated in Equation (1)

$$\Delta w_f/w_f = 2h/D_p = 0.551\sigma_c/BH \quad (1)$$

h is the depth of penetration of a single layer of proppant, D_p is the average diameter of proppant, and σ_c is net closure stress.

The maximum and minimum values of net closure stress were calculated from the conditions of maximum and minimum values of the fluid pressure in the fracture. Net closure stress is

defined as the difference between minimum horizontal stress and the fluid pressure in the fracture.

$$\sigma_c = \sigma_{hmin} - p \quad (8)$$

The minimum net closure stress occurs when the fluid pressure in the fracture is maximum or during well shut-in where the pressure is equal to reservoir pressure. The maximum net closure stress would occur when the drawdown pressure reduces the fluid fracture pressure to 0 psi. The minimum horizontal stress was calculated using the closure stress gradient of 0.523 psi/ft. Reservoir pressure was based on the 0.45 psi/ft reservoir pressure gradient. The results of proppant embedment are displayed in Table 7. (Note that 1422 psi = 1 kg/mm^2.)

Observations/Discussion

1. The L/D ratios of the core plugs tested for elastic constants were significantly less than the ASTM recommended ratio of 2:1. Consequently, biases may have been introduced in the measurements toward high CS and stiffness values.
2. Unusual axial and radial strain response was observed in cores 4a and 4b during the initial hydrostatic ramp phase of the triaxial testing. As an example, Figure 6 shows a graph of core #4b during this phase. The graph displays individual curves of the axial and radial strain, confining pressure, and axial deviatoric stress versus time. This figure shows increasing axial and radial strain (inferring reduction in length and diameter) as confining and axial stress was increased. At about 380 seconds into this segment of the test, a sudden extension in both the diameter and length appears to have occurred. This phenomenon was rarely or ever observed in the past, but may have been due to a rupture in, or extrusion of the protective sleeve near the core-steel platen interface. A sudden increase in axial load, due to the confining fluid, may have caused the axial actuator to retract a small amount in an attempt to maintain constant deviatoric stress of 200 psi. This effect was not observed when testing cores #7 and #13.
3. Core #15 was a silt/shale rock type that was not tested because it fell apart after immersion in the formation brine. There was no observed dissolution of solids, only a set fractured rock, whose remnants are shown in Appendix III.
4. Young's modulus varied between 0.74×10^6 psi to 1.19×10^6 psi among cores #4 (conglomeritic sandstone) and #7 (pebble conglomerate). The highest modulus was in core #13 ($E = 3.2 \times 10^6$ psi), which was the well-indurated, clay-rich, fine-grained sandstone. This core also had a compressive strength about 3 times greater than the other two rock intervals.
5. Figures 1 and 2 show little or no significant effect (as suggested by the overlap of the standard deviations) of either fluid on the initial hardness oil-stained sandstone in the Upper Hemlock.
6. Figures 3 and 4, also indicate little or no adverse effect of SpectraStar and Synoil on the initial hardness of the pebble conglomerate in the Lower Hemlock. Figure 4 does show, however, fresh water reducing hardness by 50%.
7. Figure 5 also indicates little or no effect of either fluid on the formation hardness of cobble conglomeritic rock.
8. The formation hardness shows a tendency to increase from the softer well sorted sandstone in Upper Hemlock (BH = 28-35 kg/mm^2) to BH = 50-100 kg/mm^2 in the

pebble conglomerate to BH = 100 – 150 kg/mm^2 in the cobble conglomerate (Lower Hemlock).

9. Because the immersion fluid had minimal observable effect on hardness, proppant embedment will likely, based on these test results, by controlled by the in-situ formation hardness and drawdown pressure applied to the fracture during production. Table 7 shows that the softer Upper Hemlock sandstone is expected to see the greatest amount of embedment. At maximum drawdown pressure, total embedment of a single layer or greater of proppant is expected to vary from 16% to 22% of the diameter of proppant. Proppant embedment in the pebble conglomeritic rock is expected to vary between 7% and 15% of the proppant diameter. The cobble conglomeritic rock only experience embedment of 3% - 4.5% of the diameter of the proppant. For proppant loadings of 1 lb/ft^2 to 4 lb/ft^2, embedment should have minimal impact on fracture conductivity. Embedment will have a much greater adverse effect at partial monolayer proppant concentrations.
10. All cores were observed to absorb water over time. The weight of water uptake is shown in the table in Appendix V.

Table 5
Static Elastic Properties of Hemlock Formation Cores*

Formation	Core Depth (ft)	Sample ID	Poisson's Ratio	Young's Modulus ($1x10^6$ psi)	C.S. (psi)
U. Hemlock	14551.0	4a	0.244	0.737	nd
		4b	0.425	1.02	9983
L. Hemlock	14848.2	7	0.290	1.19	10595
L. Hemlock	15002.7	13	0.243	3.20	29176

*Core #15 broke apart after immersion in the synthetic formation brine.

Table 6
Initial and Final Values of Formation Hardness (BH)

Core Depth (ft)	Sample ID	Initial Values*		Fluid	Final Values		% ΔBH
		BH (kg/mm^2)	Std. (kg/mm^2)		BH (kg/mm^2)	Std. (kg/mm^2)	
14492.3	2a	28.6	1.4	tap water	24.4	2.39	-14.5
	2b	26.5	3.6	SpectraStar	32.9	5.61	24.3
	2d	32.8	6.0	Synoil	25.0	3.92	-23.7
14551.0	4a	28.8	8.3	tap water	26.0	6.70	-9.6
	4b	35.5	-	SpectraStar	28.5	4.07	-19.8
	4d	31.6	9.6	Synoil	33.2	3.7	4.9
14801.8	6b	43.6	8.7	tap water	36.4	8.28	-16.4
	6c	40.4	6.0	SpectraStar	59.5	6.65	47.2
	6a	43.8	8.1	Synoil	48.1	6.34	9.9
14848.2	7a	100	15.7	tap water	49.0	16.0	-50.9
	7b	55.3	23.3	SpectraStar	44.5	6.55	-19.5
	7d	74.3	21.7	Synoil	74.6	13.9	0.4
14905.0	8	40.6	13.3	SpectraStar	56.1	1.57	38.4
14940.0	11a	108	11.0	SpectraStar	131	63	21.7
	11d	149	38	Synoil	160	32	7.4
	11b	106	18.3	SpectraStar	124	16	17.0

*measurement taken after few hours in fluid at 72 ^oF.

Table 7
Estimates of Proppant Embedment

Sample ID	Immersion Fluid	Min. Net Closure* Stress (psi)	Max. Net Closure Stress (psi)	$2h/D_p$ (min.)	$2h/D_p$ (max.)
2a	tap water	1058	7579	0.017	0.218
2b	SpectraStar	1058	7579	0.012	0.162
2d	Synoil	1058	7579	0.016	0.213
4a	tap water	1062	7610	0.016	0.206
4b	SpectraStar	1062	7610	0.014	0.188
4d	Synoil	1062	7610	0.012	0.161
6a	Synoil	1081	7741	0.009	0.113
6b	tap water	1081	7741	0.011	0.149
6c	SpectraStar	1081	7741	0.007	0.091
7a	tap water	1084	7766	0.009	0.112
7b	SpectraStar	1084	7766	0.009	0.123
7d	Synoil	1084	7766	0.006	0.073
8	SpectraStar	1088	7795	0.008	0.098
11a	tap water	1091	7814	0.003	0.042
11b	Synoil	1091	7814	0.003	0.044
11d	SpectraStar	1091	7814	0.003	0.034

*net closure based on σ_{hmin} gradient of 0.523 psi/ft and reservoir pressure gradient of 0.45 psi/ft

Figure 1
Initial//Final Formation Haradness of Cores #2 (Upper Hemlock)

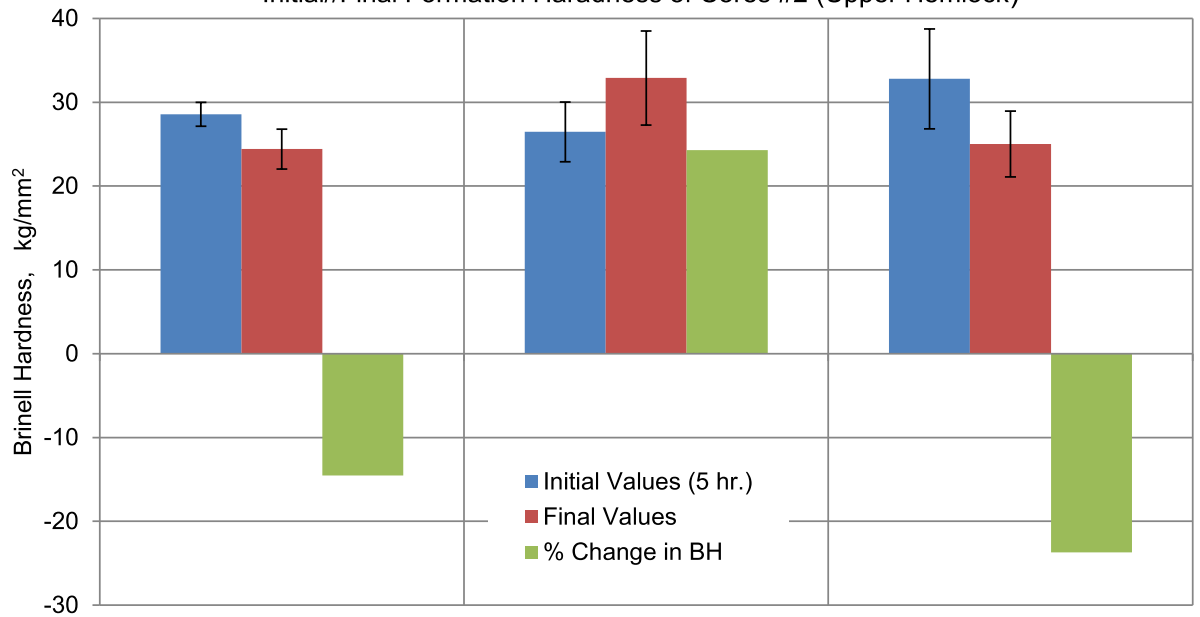

Figure 2
Initial/Final Formation Hardness of Cores #4 (Upper Hemlock)

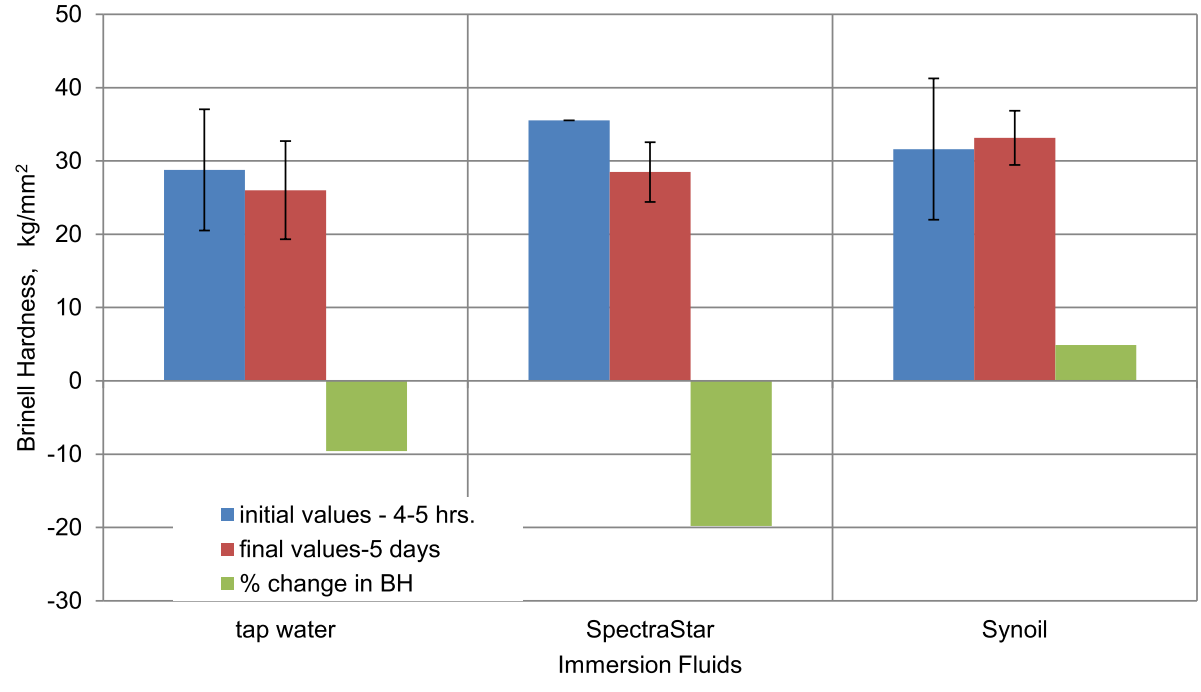

Figure 3
Initial/Final Formation Hardness of Cores #6 (Lower Hemlock)

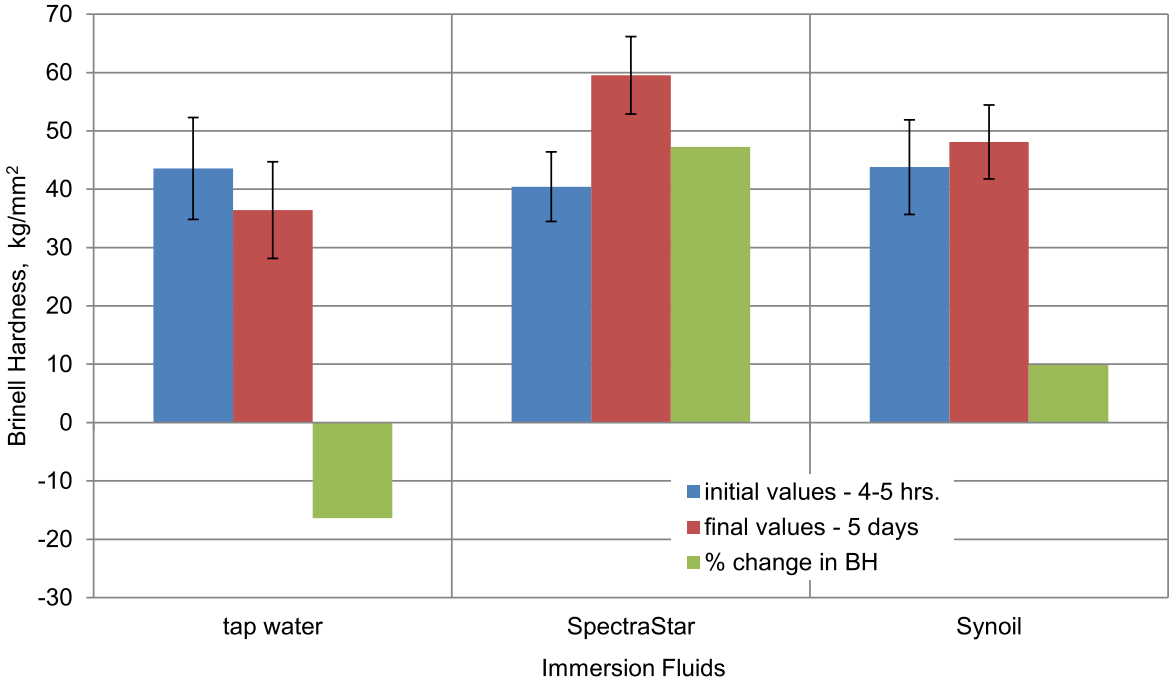

Figure 4
Initial/Final Formation Hardness of Cores #7 (lower Hemlock)

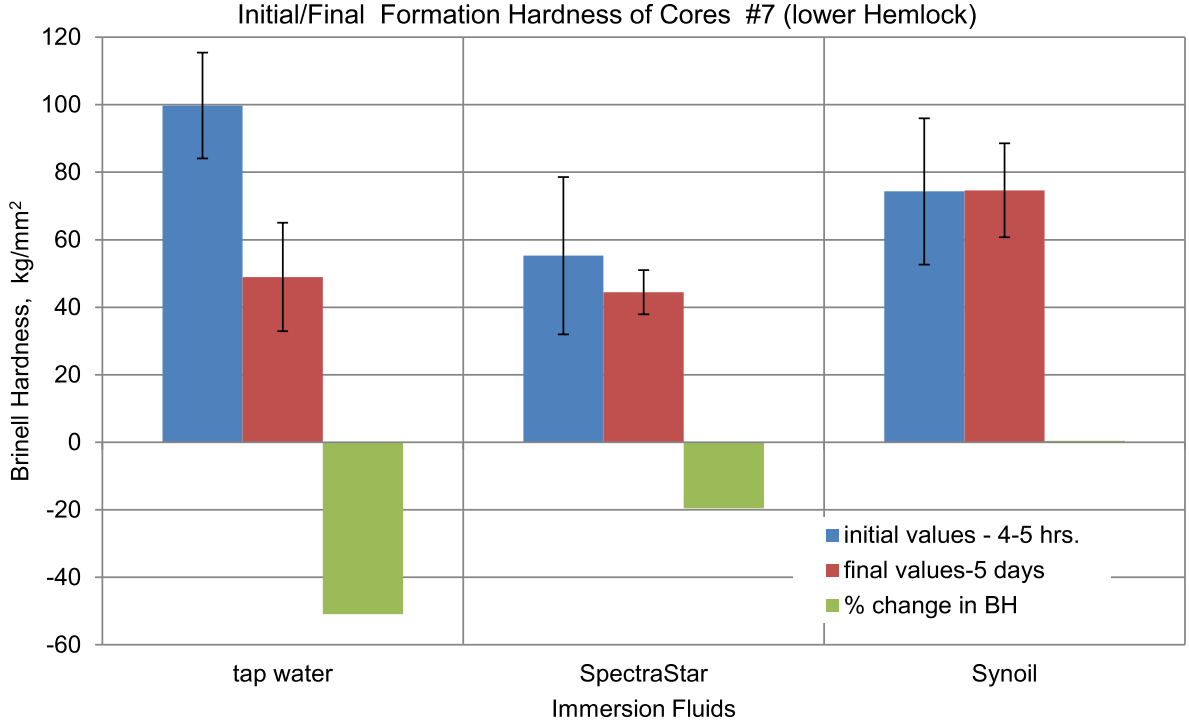

Figure 5
Initial/Final Formation Hardness of Cores #11 (Lower Hemlock)

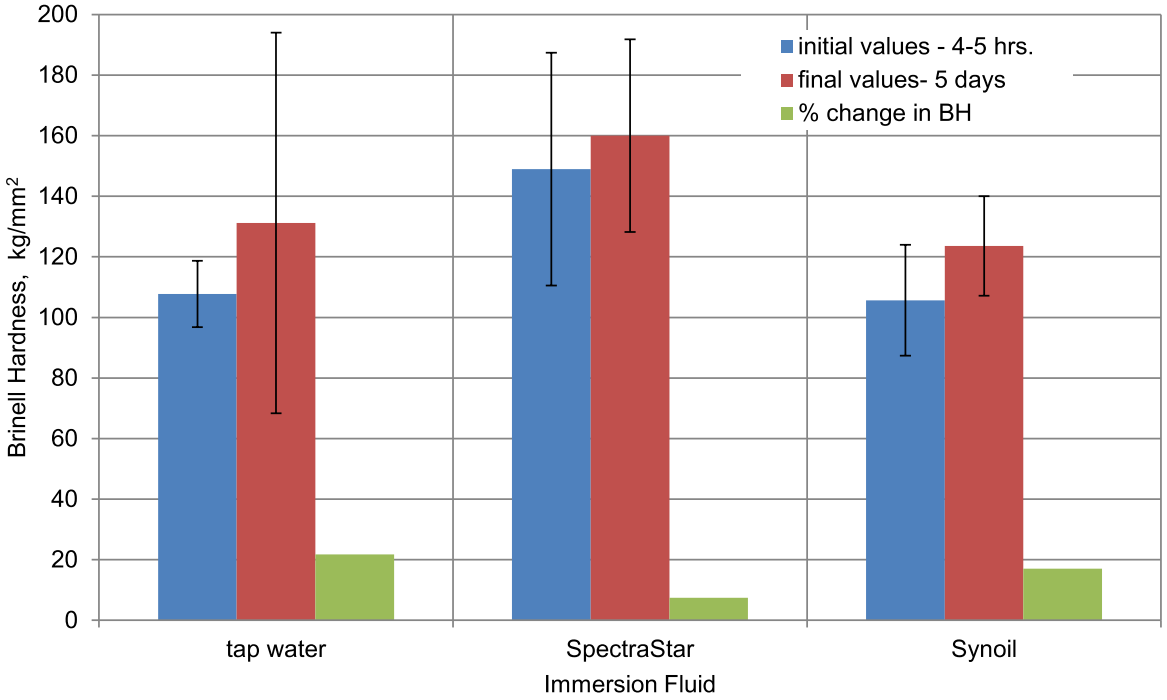

Figure 6: Core #4B
Sudden Bulk Volume Expansion During Hydrostatic Ramp Phase

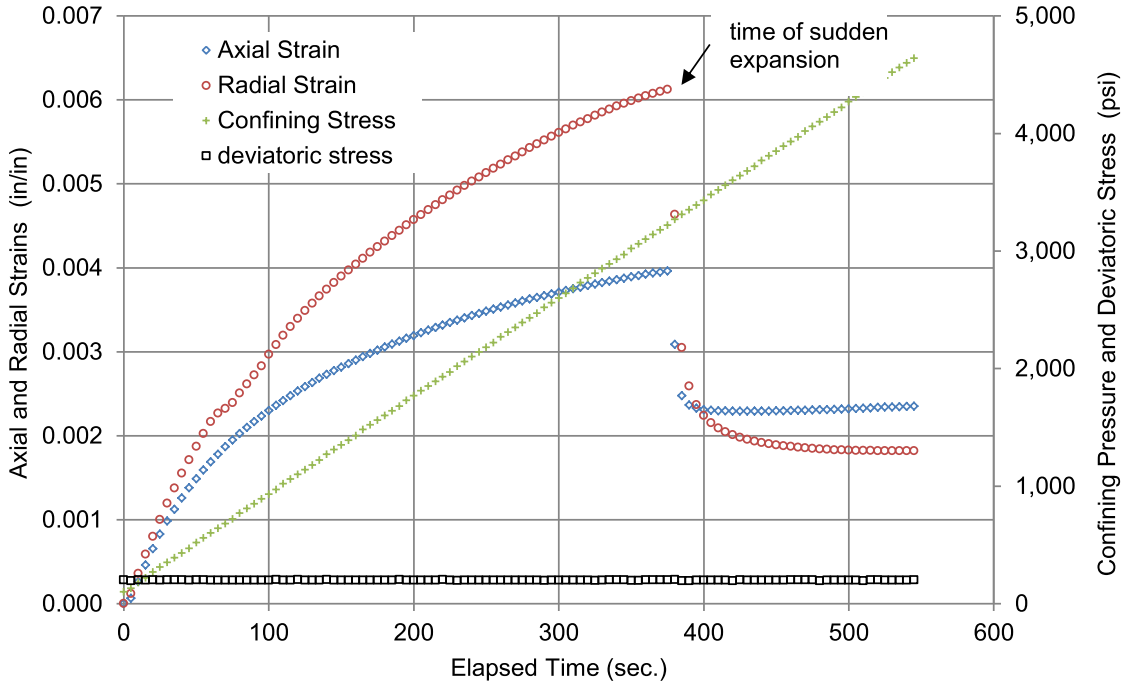

APPENDICES

Appendix I: Test Procedures

Sample Preparation

The one-diameter cores were prepared by grinding the ends flat and parallel to each other to within a tolerance of 0.001-inch. The newly drilled samples were extracted as a batch using a low boiling point solvent. The newly drilled samples were extracted as a batch using a low boiling point solvent. All samples were dried to stable weights in a low temperature (150°F) convection oven[2].

Core plugs were then vacuum saturated with prepared synthetic formation brine. Tests were conducted at 72 °F.

Triaxial Tests

Testing procedures and apparatus closely followed ASTM recommended practices[4]. Triaxial or confined tests were performed on a GCTS™ hydraulic test frame. Core samples were sleeved in thin polyolefin heat-shrink tubing (0.017-inch thick) and mounted between two steel platens. The spherical seat of the upper platen contacted an internal pressure-compensated load cell (100 thousand pound load capacity).

Two LVDT's were positioned parallel to the length of the core sample (and internal to the pressure vessel) and used to measure the change in sample length. A chain-type displacement gauge holding a third LVDT was wrapped around the circumference of the core and used to measure the change in circumference of the core. Confining stress was supplied by hydraulic oil that fills the vessel and pressurized using a programmable pump. Tests were conducted under "drained" conditions by keeping the pore pressure lines open to atmospheric pressure. All tests were conducted at room temperature (72 °F).

The stress path consisted of an initial hydrostatic stress to reservoir net mean stress followed by a wait time to allow the radial and axial strains to come into equilibrium with the applied load. Afterward, the confining pressure was held constant while the axial stress went through two load/unload cycles. The amplitude of the 1st stress cycle was to yield stress, which was defined as the point at which volume strain curve began showing signs of reaching its maximum value. The 2nd stress cycle was taken to failure and beyond to observe post-failure behavior. The axial deviatoric stress was ramped at a constant strain rate of 0.05%/minute. The cores were then unloaded and photographed.

The axial deviatoric stress was calculated from the ratio of axial force to sample cross-sectional area (corrected for dilation). The uncorrected axial strain was calculated from the ratio of the average displacements of the two axial LVDT's to the initial sample length.

The total axial deformation included some deformation from the steel platens to which the axial LVDT rings were held in place. The axial strain was corrected by subtracting out the effect of the platens using the relationship:

$$\varepsilon_c = \varepsilon_m - \Delta\sigma\, A_c/(Lb) \qquad \text{(I-1)}$$

ε_m is measured strain, $\Delta\sigma$ is the change in axial stress, A_c is the sample corrected cross-sectional area, L is the initial sample length, and "b" is the compliance of the platens, defined as $\Delta F/\Delta x$, where ΔF is the force required to cause a displacement, Δx, in the platens. The "b" compliance factor was actually determined for each deviatoric stress path by measuring the Young's modulus (E_{ap}) of an aluminum standard (E_{st}) whose elastic properties are known. "b" was then inferred from the expression:

$$1/E_{st} = (1/ E_{ap}) – A/(Lb) \quad \text{(I-2)}$$

$$b = AE_{ap}E_{st}/(L\{E_{st}-E_{ap}\}) \quad \text{(I-3)}$$

A is the cross sectional area of the standard and L is the length of the standard. The "b" compliance factor was determined over each of the deviatoric stress intervals at which the Young's modulus is calculated.

Young's modulus (E) was calculated from a linear least-square regression of the increasing axial stress versus axial strain curve of the 2nd cycle between 0% and 50% of peak strength.

$$E = \Delta\sigma/\Delta\varepsilon_c \quad \text{(I-4)}$$

The radial strain was expressed as:

$$\varepsilon_r = -\gamma\Delta C/(\pi D) \quad \text{(I-5)}$$

ΔC is the change in circumference of the sample, which is directly measured by the circumferential LVDT. Note that an increase in circumference (i.e. positive ΔC) produces a negative radial strain. D is the sample's initial diameter. γ is a geometrical correction factor required[4],[5] when using chain-type gauges that measure chord length and not arc length. The Poisson's Ratio was calculated from the linear least square regression of the radial versus axial strain curve over the same axial strain interval used to calculate Young's modulus. Another criterion for evaluating the elastic constants was that the stress-strain interval should be confined to the interval prior to reaching maximum volume strain reduction (see Appendix II).

$$\nu = -\Delta\varepsilon_r/\Delta\varepsilon_c \quad \text{(I-6)}$$

The volumetric strain ($\varepsilon_a + 2\varepsilon_r$) was monitored during application of the deviatoric stress paths. The volume strain was monitored to detect the onset of deviation from linear response. Once detected, the axial stress was reduced back to within 200 psi of the confining stress, and 2nd axial deviatoric stress cycle was initiated. The peak in the volume versus axial strain curve was also used to limit the interval over which the elastic constants were evaluated.

Test Conditions/Apparatus for Triaxial Testing of Rock

Mechanical Test Apparatus	GCTS Hydraulic Press
Load Cell	100 kip Tovey
Confining Stress	4675 psi
Test Temperature	Room (72 ^{o}F)
Fluid Saturant	Formation Brine
Pore Pressure	atmospheric
Displacement Gauges	MacroSensor LVDT's
Stress/Strain Rate Control	0.05%/minute strain rate
Number of Deviatoric Stress Cycles	2
Where Moduli Calculated	0%-50% of peak stress of 2nd cycle
ASTM Practice	ASTM D 7012-07

Brinell Hardness Testing

Brinell hardness is measured using an ELE™ steel ball penetrometer. The device consists of a single steel ball attached to a stationary plate and rod. The core sample to be tested sits on pedestal beneath the steel ball. A calibrated load-ring is connected in series with the steel ball and plate and measures the load at the steel ball/core interface as the sample is raised up against the steel ball. Ball diameters are typically 0.061-inches and 0.125-inches depending on grain size. A micrometer is used to measure the displacement, h, of the steel ball as is penetrates the core sample.

Brinell Hardness (BH) is defined as the ratio of load (force) to the contact area of the indentation from the steel ball (ASTM E10-10).

$$BH = F/A_c \quad \text{(I-7)}$$

The contact area, A_c, is calculated from the expression:

$$A_c = \pi D_b h \quad \text{(I-8)}$$

The penetration distance, h, was measured directly using a calibrated micrometer.:

The BH values at three to four different locations on core surface are typically measured and averaged to obtain the average BH value and standard deviation of the core.

Attempts were made to measure BH at the same hardness scale, F/D^2 (see table below). F is the force on the ball and D is the diameter of the ball. ASTM emphasizes that comparisons of BH between cores or within a core are strictly valid only when the hardness scale used in the tests are all the same.

Summary of Test Procedures

Test Equipment	ELE
Ball Diameter	0.061-inch (1.55 mm)
Test Temperature	72 °F
Immersion Fluids	See Table 1
Immersion Temperature	190 °F
Immersion Time	Up to 5 Days
Allowed relaxation time	15 seconds
Hardness scale (F/D^2) kg/mm^2	5.78
ASTM standard	E10-10

Estimating Proppant Embedment

The following section presents the derivation for estimating proppant embedment from post-immersion Brinell hardness measurements. The calculation was based on a simple model of a single layer of non-deformable proppant arranged in a hexagonal close-pack array pressed between the surfaces of a smooth fracture.

Brinell hardness (BH) is defined by the following relationship.

$$BH = F/A_c = F_i/(\pi D_p h) \quad \text{(I-11)}$$

F is the average force per proppant particle. A_c is the area of contact that a single embedded particle makes with the rock. D_p is the average diameter of the proppant grain and h is the embedment of the proppant. The contact area, by definition, is equal to the quantities in the denominator of Equation (I-11). The average force per particle is equal to the net closure stress (σ_c) divided by n, the number of particles per unit area.

$$F = \sigma_c/n \quad \text{(I-12)}$$

For a 2-D hexagonal close-packed arrangement of spheres, it can be shown that:

$$n = 1.155/(D_p)^2 \quad \text{(I-13)}$$

Solving for h in Equation (I-11) and substituting Equations (I-12) and (I-13) for F and n, respectively, the following expression for h is obtained:

$$h = \sigma_c\, D_p/[1.155(\pi)BH] \quad \text{(I-14)}$$

The fractional reduction in initial fracture width of a monolayer of proppant is defined as:

$$\Delta w_f/w_f = 2h/D_p \quad \text{(I-15)}$$

The term $2h/D_p$ comes about from the fact that the initial fracture width is equal to the average diameter of a proppant grain (i.e. $w_f = D_p$), and the change in fracture width is due to proppant embedment into both faces of the fracture, 2h.

Substituting Equation (I-14) into (I-15) for h, the fractional change in initial fracture width can be reduced to an expression involving only BH and net closure stress:

$$\Delta w_f/w_f = 0.551\sigma_c/BH = 2h/D_p \quad \text{(I-16)}$$

Note that 1422 psi = 1 kg/mm^2.

Appendix II – Stress-Strain Curves from Triaxial Testing

The following pages contain the stress-strain curves from which Young's modulus and Poisson's Ratio were calculated. Each page contains two figures for a single core plug: (1) top figure – axial stress versus axial strain that was used to determine Young's modulus; (2) bottom figure – radial strain versus axial strain that was used to determine Poisson's Ratio. The bottom figure also displays the volume strain versus axial strain. This curve was used to place an upper limit to the axial strain over which the elastic constants were determined. All constants were calculated over an axial strain interval prior to reaching the maximum reduction in the volume strain.

The portion of the curve used to determine Young's modulus and Poisson's Ratio is shown in "red". The values of the moduli are also displayed in the figures. Note that the strains were set equal to zero at the start of the 1st axial deviatoric load cycle. The elastic moduli were calculated from the increasing axial load of the 2nd cycle between 10% - 50% peak strength (where possible). Confining stress equaled 4675 psi.

Note that 1 Mpsi = 1x10^{6} psi = 6.897 GPa.

Figure II-1
Young's Modulus of Core #4A - 2nd test (2000 psi confining)

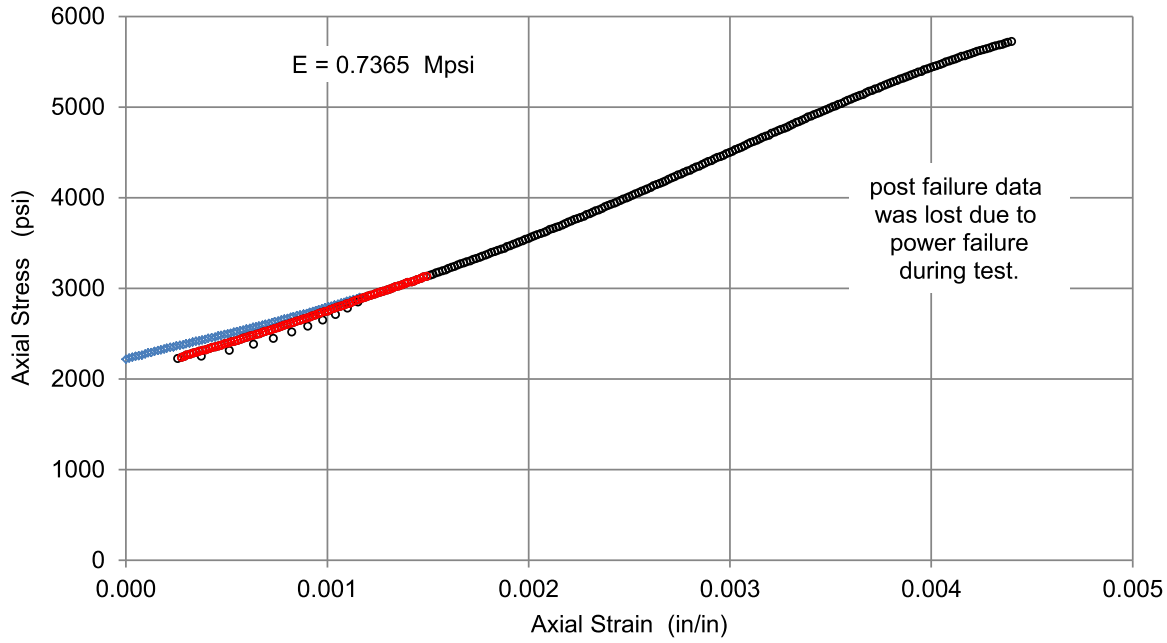

Figure II-2
Poisson's Ratio of Core #4A

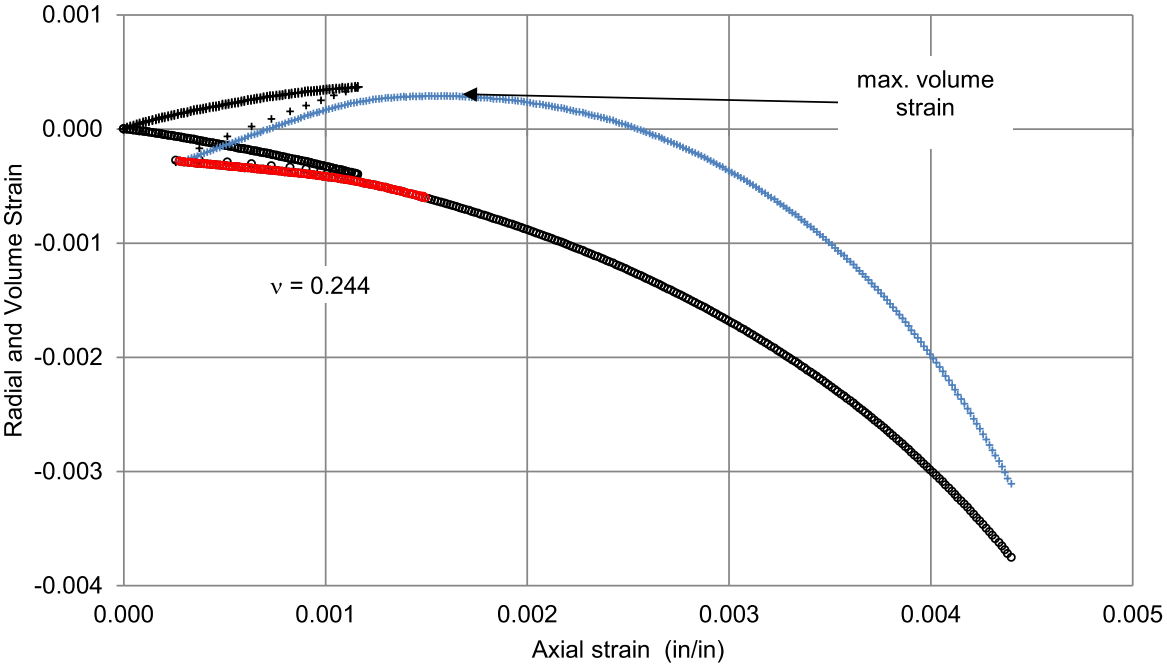

Figure II-3
Young's Modulus of Core #4B - 4675 psi confining

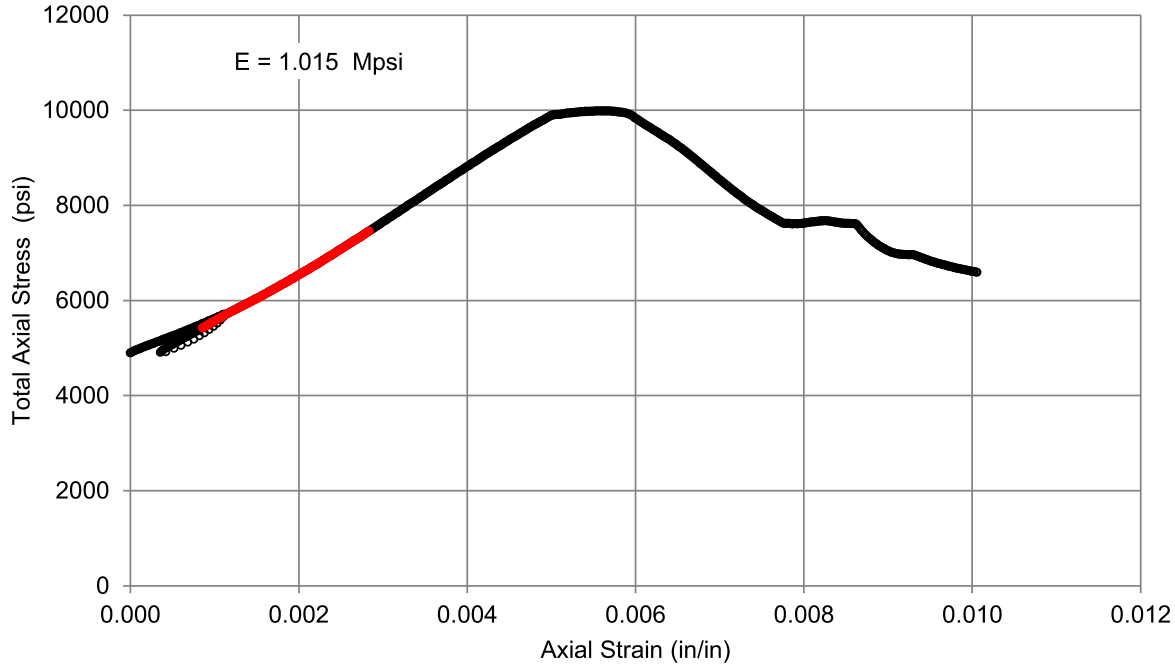

Figure II-4
Poisson's Ratio of Core #4B

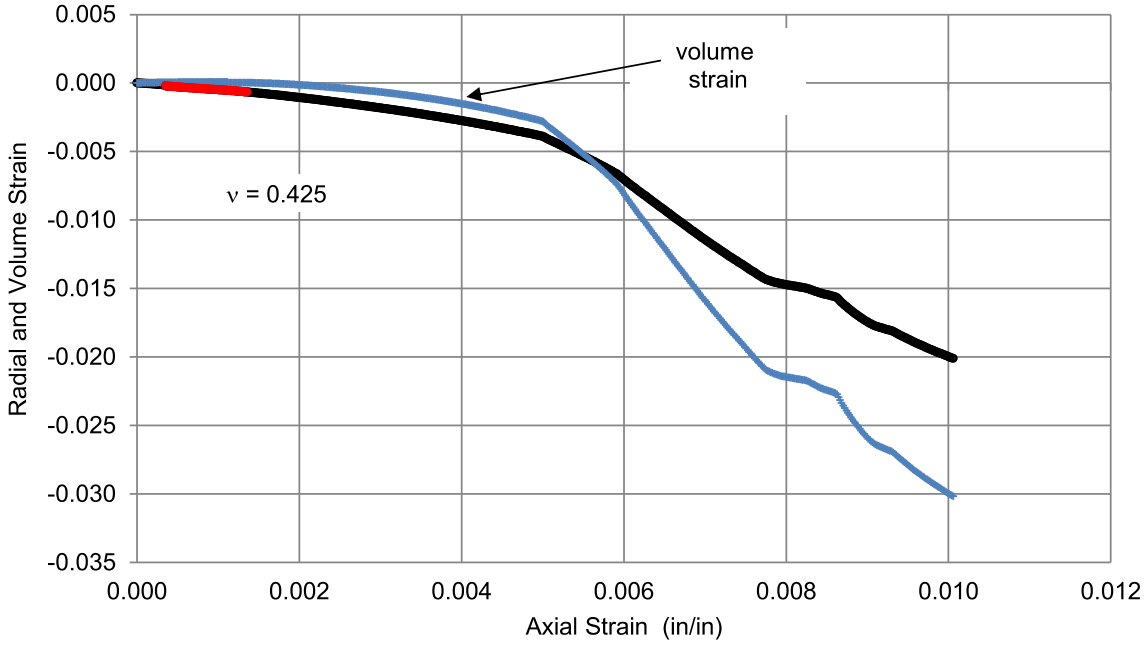

Figure II-5
Young's Modulus of Core #7 - 4675 psi confining

CS = 10595 psi

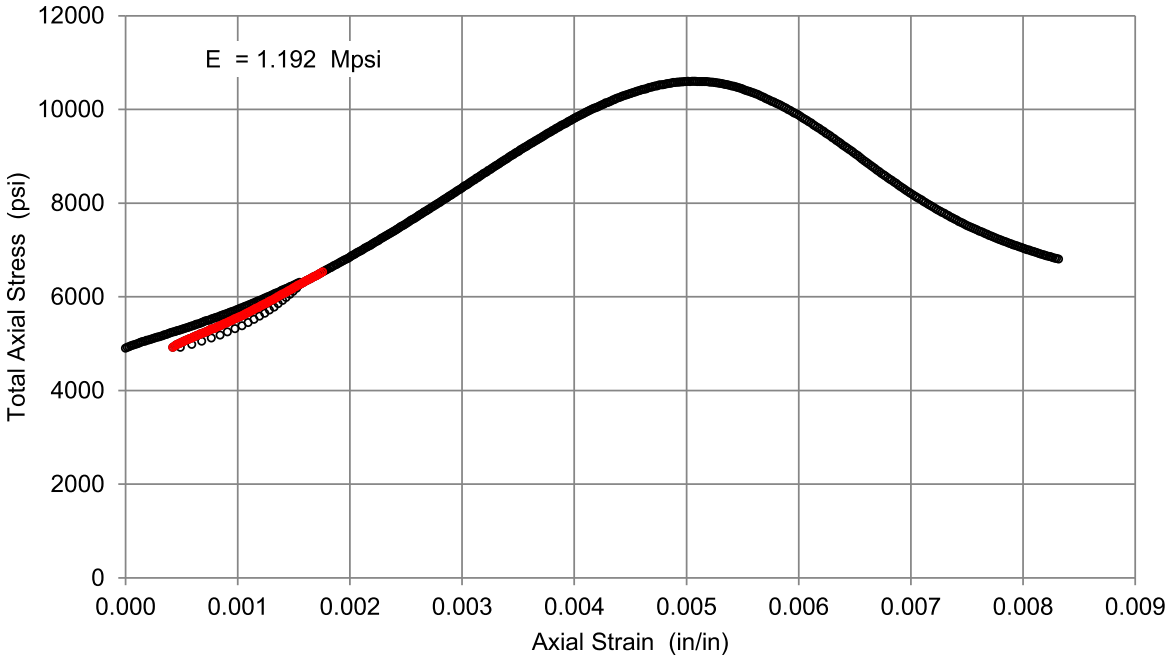

Figure II-6
Poisson's Ratio of Core #7

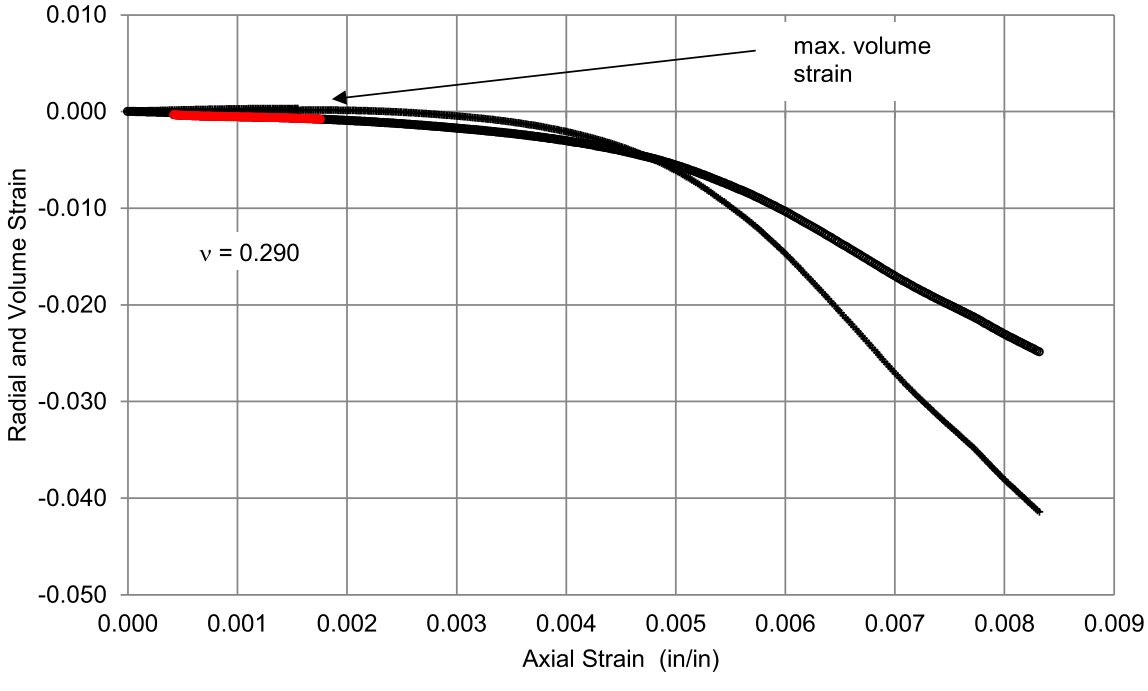

Figure II-7
Young's Modulus of Core #13 - 4675 psi confining

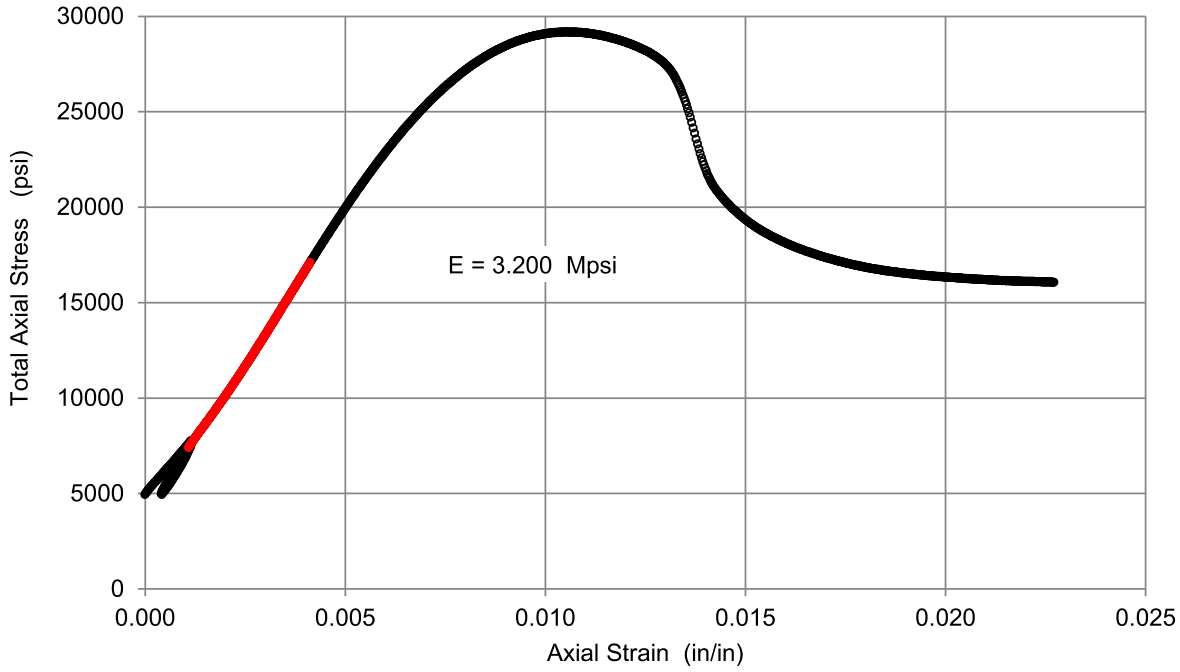

Figure II-8
Poisson's Ratio of Core #13

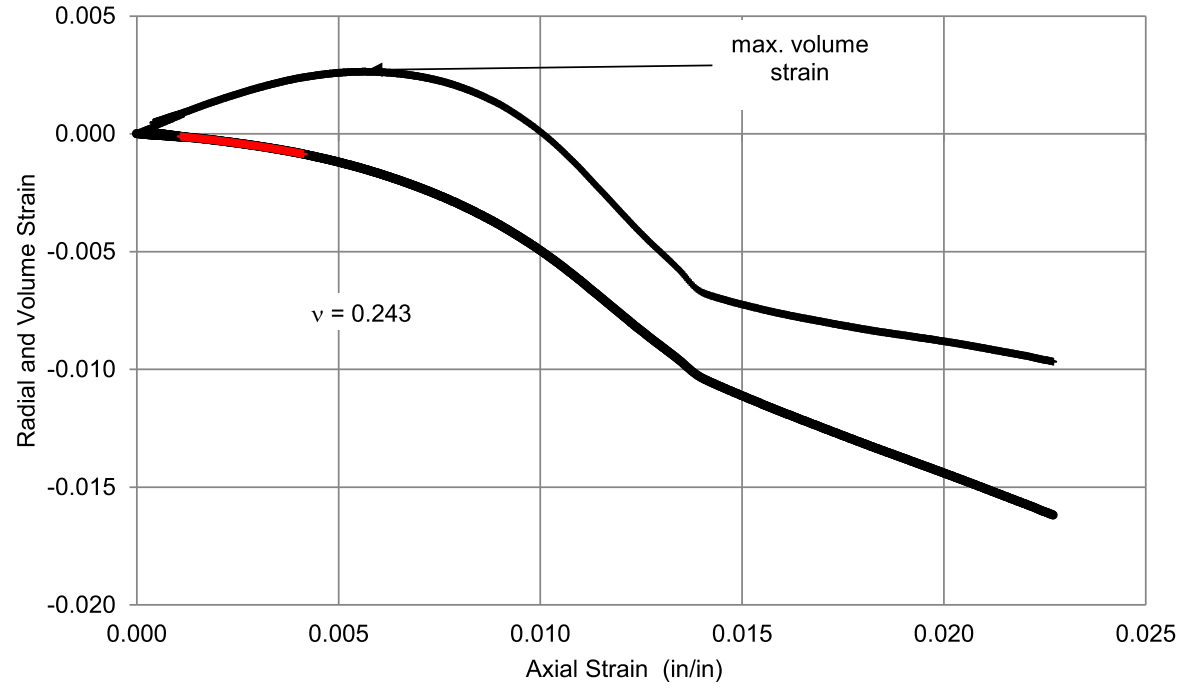

Appendix III – Pre/Post Failure Core Photographs

This section contains photographs of core plugs that were tested for elastic properties and strength before and after testing.

Before Triaxial Testing – Side Views

End Views

Core #15 after Immersion in Formation Brine

Appendix III – Pre/Post Failure Core Photographs

Post-Failure Photographs

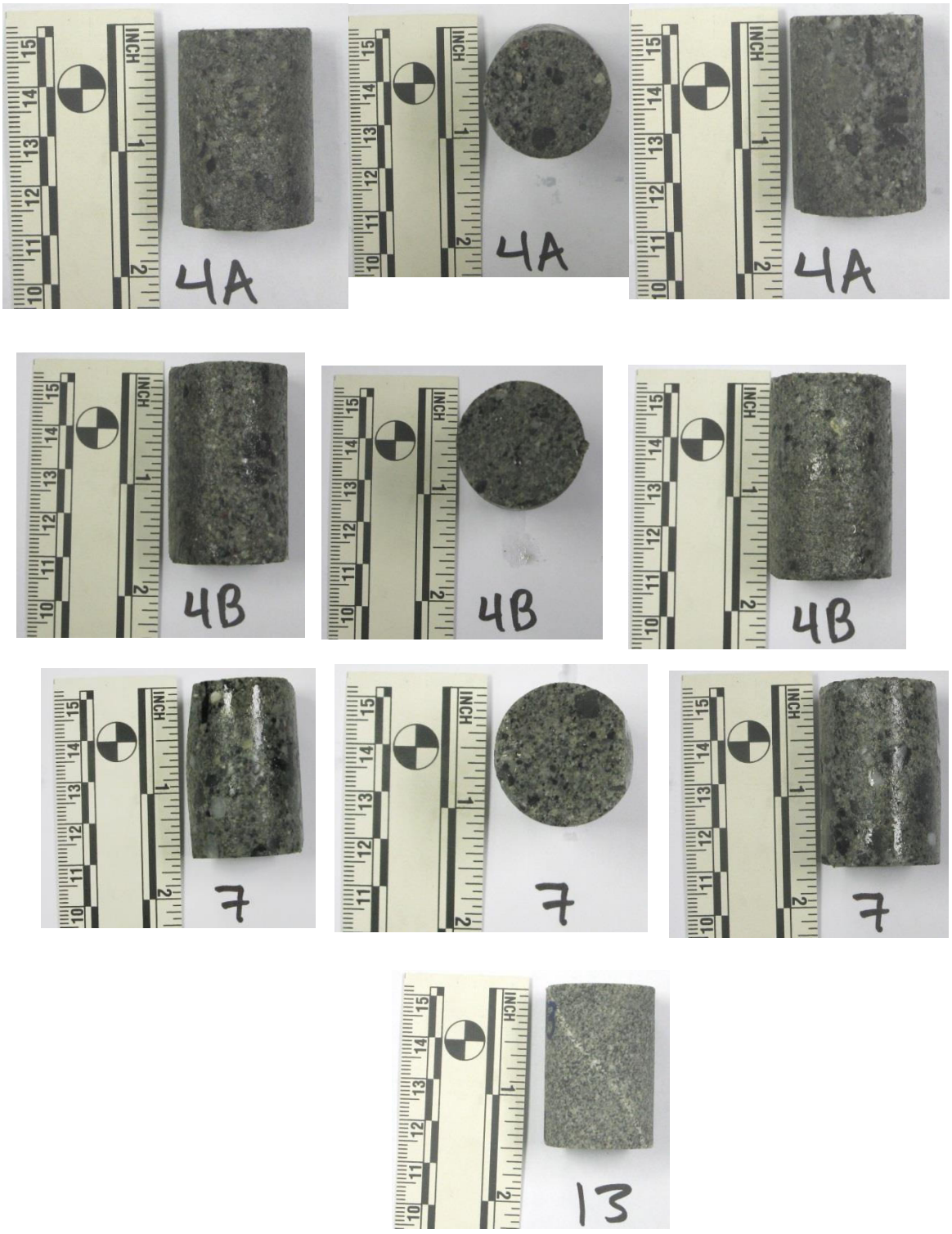

Appendix IV –Photographs of Core Samples (Pre-Immersion)

This section contains photographs of core samples that were used for immersion testing, prior to immersion.

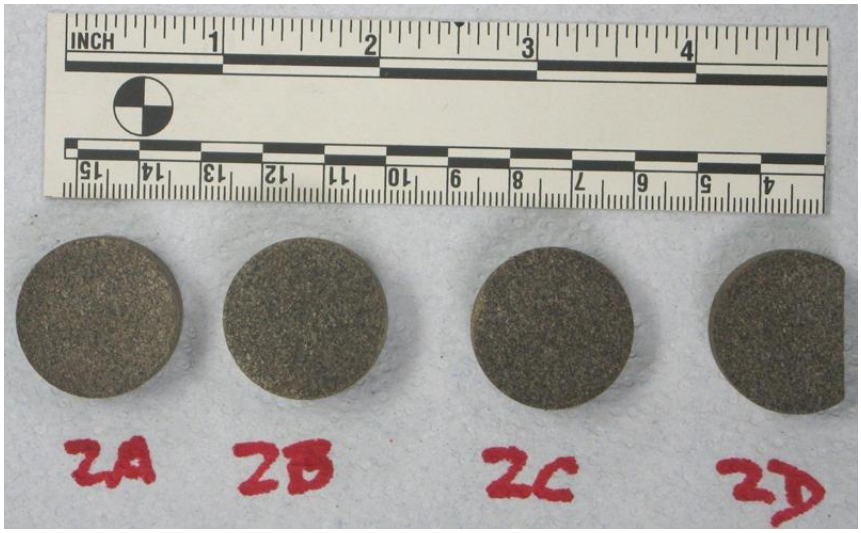

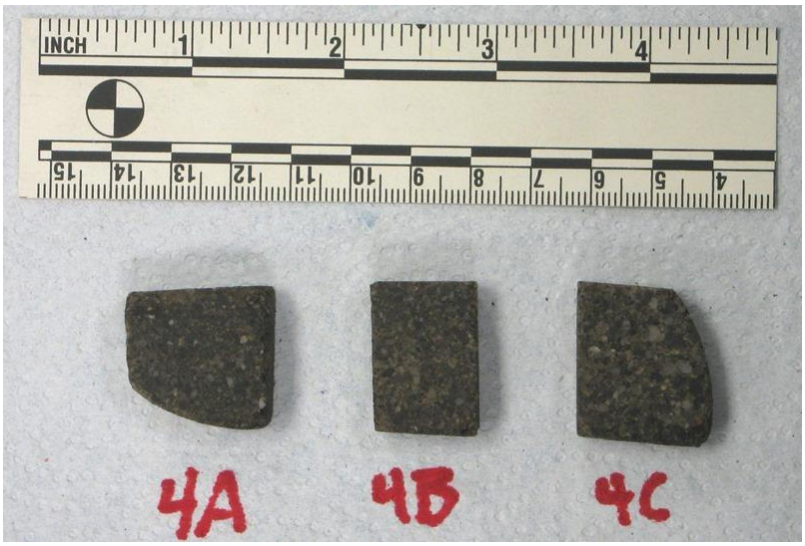

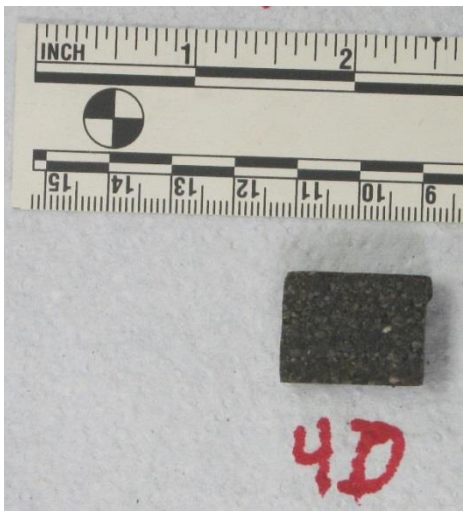

Appendix IV –Photographs of Core Samples (Pre-Immersion)

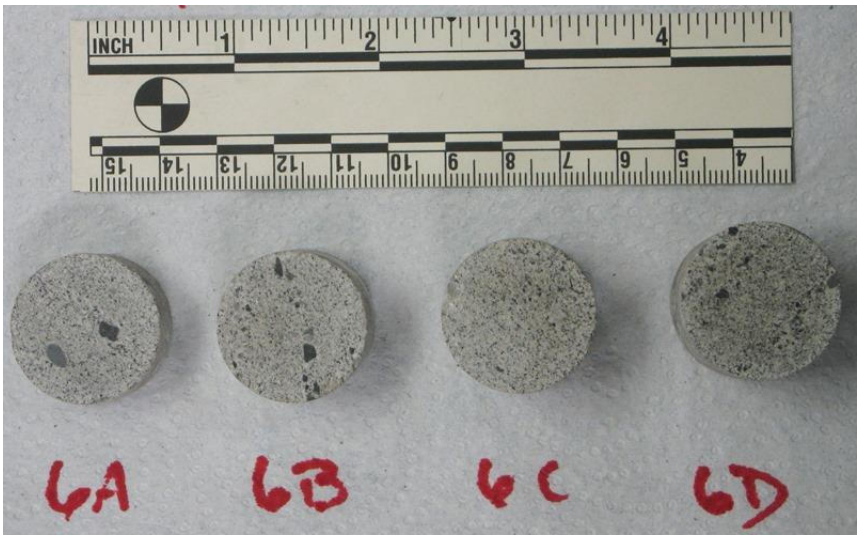

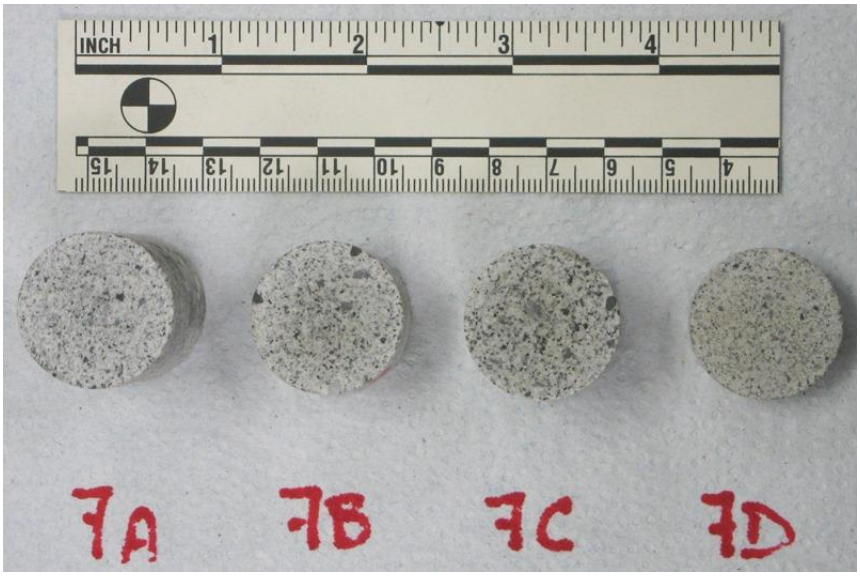

Appendix IV –Photographs of Core Samples (Pre-Immersion)

Appendix V – Increase in Weight of Core Plugs During Immersion

The data in Table V shows the weight and changes in weight of each core plug by absorbing the immersion fluid. The initial dry weight, weight after a few hours immersed at room temperature, and final weight after 4-5 day immersion are shown. The Brinell hardnesses (see Table 6) were also measured after the early and final immersion times. No BH measurements were taken on the dry core samples. Results showed an increase in weight at each time interval. The changes in weight were calculated from the difference between weight after immersion and the initial dry weight.

Table V
Weight of Core Plugs vs. Immersion Time

Sample ID	Immersion Fluid	Initial Wt. (dry)	Immersion Time @ 72 °F (hrs.)	Wt. (gm.)	ΔWt. (gm)	Total* Immersion time (hrs.)	Wt. (gm.)	ΔWt. (gm)
2a	tap water	12.256	6.00	12.319	0.063	124.58	12.709	0.453
2b	SpectraStar	15.609	6.42	15.694	0.085	125.00	16.066	0.457
2d	Synoil	8.075	0.83	8.183	0.108	94.25	8.306	0.231
4a	tap water	10.509	3.08	10.573	0.064	121.67	10.789	0.280
4b	SpectraStar	8.876	6.50	8.923	0.047	125.08	9.151	0.275
4d	Synoil	8.898	0.83	8.952	0.054	94.25	9.069	0.171
6a	Synoil	17.299	0.83	17.428	0.129	94.25	17.555	0.256
6b	tap water	23.449	5.92	23.727	0.278	124.50	23.871	0.422
6c	SpectraStar	31.253	7.50	31.617	0.364	126.08	31.855	0.602
7a	tap water	39.317	5.75	39.575	0.258	124.33	39.663	0.346
7b	SpectraStar	23.712	7.58	23.843	0.131	126.17	23.895	0.183
7d	Synoil	13.712	0.83	13.773	0.061	94.25	13.81	0.098
8	SpectraStar	27.667	7.75	27.901	0.234	128.42	28.181	0.514
11a	tap water	12.099	6.08	12.119	0.020	126.75	12.124	0.025
11b	Synoil	7.424	0.83	7.439	0.015	94.25	7.451	0.027
11d	SpectraStar	9.091	7.92	9.105	0.014	128.58	9.117	0.026

*total time = immersion time at 72 °F + immersion time at 190 °F.

REFERENCES

[1] BHI TSR No. T14-12-1209, “Analysis of Core Plugs and Whole Core Segments”, by M. Wilson and BJ Davis, Jan. 19, 2015.

[2] BHI TSR No. T-14-12-1209, “Rock:Fluid Compatibility – Regain Permeability”, by J. Cutler, Jan. 13, 2015.

[3] Water analysis report from Core Laboratories (2001) was supplied by the client.

[4] ASTM D 7012-07, “Standard Test Method for Compressive Strength and Elastic Moduli of Intact Rock Core Specimens under Varying States of Stress and Temperatures”.

[5] Appendix D – “Circumferential Extensometer Strain Calculation”, MTS Rock and Concrete Mechanics Testing Systems, Version 7, April 1998.

[6] ASTM E10-10, “Standard Test Method for Brinell Hardness of Metallic Materials”

Technology Center Report No.	**T-14-12-1209**
Reported by:	R. Maharidge, Ph.D.
Requested by:	Edwin Post
Location:	Kenai, Alaska
Participants:	Rolando Lew – Sample Preparation and Triaxial Testing R. Maharidge – Immersion Testing and Reporting
Distribution:	Edwin Post, Kenneth Nix, Joshua Herald, Robert Hurt, David Susko, BJ Davis, TTC File.

The above data is supplied solely for informational purposes, and Baker Hughes makes no guarantees or warranties, either expressed or implied, with respect to the accuracy or use of these data and interpretations. All product warranties and guarantee shall be governed by the standard contract terms at the time of sale.

T-14-12-1209
Analysis of Coreplugs & Wholecore Segments

Pressure Pumping Technology Center, Tomball

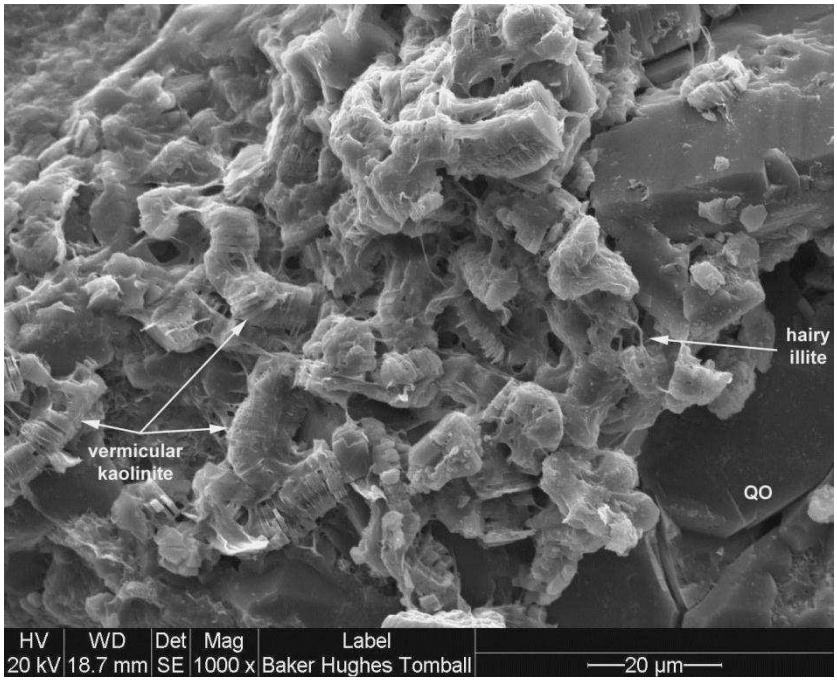

14905': pore-filling vermicular kaolinite with late diagenesis hairy illite

COOK INLET ENERGY LLC
REDOUBT UNIT WELL #02; REDOUBT UNIT FIELD
COOK INLET BASIN
KENAI PENNINSULA BOROUGH, ALASKA
API# 50-733-20501-0000
HEMLOCK FORMATION

TECHNICAL REPRESENTATIVE:
EDWIN POST, KENAI, ALASKA

FEBRUARY 06, 2015

© 2014 Baker Hughes Incorporated. All rights reserved. This report may contain confidential customer information and should not be discussed, provided to or otherwise disclosed to anyone outside of Baker Hughes other than the customer or authorized customer representative.

OBJECTIVE(S)

Coreplugs and conventional wholecore segments from the subject well were submitted to the Geological Laboratories Group at the *Pressure Pumping Technology Center (PPTC)* for rock/pore properties characterization. The objectives of this analysis were to characterize framework mineralogy, cements, clays, and porosity types present in the sample, identify potential completion problems, and to make appropriate well completion recommendations. Analyses conducted were stereomicroscopy, helium porosity, air permeability, capillary suction time analysis (CST), scanning electron microscopy/energy dispersive spectrometry (SEM/EDS), and X-ray diffraction (XRD).

Brinell Hardness measurements pre- and post-immersion in selected fluids were performed in the Geomechanics Laboratory. Regained permeability measurements were conducted on suitable coreplugs in the SCAL laboratory. Results of those tests were reported separately.

SAMPLE ANALYSES

Seven coreplugs from a 2001 routine core analysis project, and eight wholecore segments from the same cored interval were shipped to Geological Laboratories in Tomball for evaluation. Table #1 on the following page details the sample depths, zonation, and provides brief lithological descriptions. Coreplugs were drilled from the wholecore segments for regained permeability testing; due to the moderate cementation of these conglomeritic samples, coreplugs could not be obtained from all of the samples.

Basic Reservoir Properties (Porosity & Gas Permeability)
Basic reservoir properties (helium porosity, air permeability, grain density) are presented in Table #2, which includes the 2001 Core Laboratories values (in parenthesis), remeasured values on coreplugs that were potential candidates for regained permeability measurements, and values measured on the newly drilled coreplugs.

Mineralogical Analysis
Sub-samples were selected for mineralogical definition by x-ray diffraction techniques (XRD). X-ray diffraction techniques are used to determine the inorganic crystalline material content of samples. Interpreted minerals and their relative percentages are shown in Table #3.

Table #1 – Sample Locations and Brief Descriptions

Zone	#	Depth	Description
Upper Hemlock	1	14429.0	Pebble conglomerate, (pebbles up to 25mm), brownish-gray matrix, black/white/gray pebbles, very poorly-sorted, moderately-indurated
	2	14492.3	Sandstone, brown (oil-stained), fine-grained, well-sorted, moderately-indurated
	3	14544.7	Pebble conglomerate, (pebbles up to 7mm), brownish-gray matrix, black/white/gray pebbles, very poorly-sorted, moderately-indurated
	4	14551.0	Sandstone, conglomeritic (pebbles up to 3mm), brown (oil-stained), poorly-sorted, moderately indurated
	5	14551.3	Pebble conglomerate, (pebbles up to 12mm), light-gray matrix, black/white/gray pebbles, very poorly-sorted, moderately-indurated
Lower Hemlock	6	14801.8	Pebble conglomerate, (pebbles up to 11mm), light-gray matrix, black/white/gray pebbles, very poorly-sorted, well-indurated
	7	14848.2	Pebble conglomerate, (pebbles up to 5mm), light-gray matrix, black/white/gray pebbles, very poorly-sorted, well-indurated
	15	?14877.3	Shale/Mudstone, dark-gray, naturally-fractured
	8	14905.0	Pebble conglomerate, (pebbles up to 20mm), brownish-gray matrix, black/white/gray pebbles, very poorly-sorted, moderately-indurated
	9	14924.3	Pebble conglomerate, (pebbles up to 9mm), light-gray matrix, black/white/gray pebbles, very poorly-sorted, moderately-indurated
	10	14925.0	Pebble conglomerate, (pebbles up to 10mm), brown (oil-stained), black/white/gray pebbles, very poorly-sorted, moderately-indurated
	11	14940.0	Cobble conglomerate, (pebbles up to 50mm), gray matrix, black/white/gray pebbles, very poorly-sorted, moderately-indurated
	12	14940.3	Pebble conglomerate, (pebbles up to 6mm), light-gray matrix, black/white/gray pebbles, very poorly-sorted, well-indurated
	13	15002.7	Sandstone, light-gray, fine-grained, well-sorted, well-indurated, clay-rich
	14	15025.7	Pebble conglomerate, (pebbles up to 11mm), light-gray matrix, black/white/gray pebbles, very poorly-sorted, well-indurated

Note: Coreplug #15 appears to have been included with the other 14 samples to represent a mudstone interbed. A CoreLab sample number of 282L appears to indicate that it is from depth 14877.3', which would place it in the shallower portion of the Lower Hemlock.

Table #2 – Sample Locations and Basic Reservoir Properties

Zone	#	Depth	Core Lab ID#	Gas Perm md.	Helium Porosity %	Grain Density gm/cc
Upper Hemlock	1	14429.0				
	2	14492.3		4.93 4.81	12.9 13.0	2.66
	3	14544.7	(115)	(138)	(12.7)	(2.65)
	4	14551.0		92.7 71.2	13.8 13.5	2.64 2.65
	5	14551.3	(122)	(30.6)	(7.5)	(2.65)
Lower Hemlock	6	14801.8		1.15 0.051	24.4 12.3	2.63
	7	14848.2		0.0201 0.0002	14.0 15.9	2.64
	15	? 14877.3	(282L)	(? 0.05)	(? 2.5)	(? 2.64)
	8	14905.0				
	9	14924.3	(313)	(68.7) 61.9	(12.8) 21.4	(2.68) 2.64
	10	14925.0				
	11	14940.0				
	12	14940.3	(325)	(10.8)	(9.6)	(2.66)
	13	15002.7	(378)	(2.05) 40.7	(11.0) 9.3	(2.65) 2.65
	14	15025.7	(401)	(17.5) 15.7	(9.4) 9.9	(2.65) 2.64

2001 Core Lab values in parenthesis; all others measured in Tomball.

Table #3 - Mineralogical Analysis (in Weight Percents)

Mineral Phases	Upper Hemlock				
	1	2	3	4	5
	14429'	**14492.3'**	**14544.7'**	**14551'**	**14551.3**
Quartz (SiO_2)	75	67	77	72	75
Plagioclase Feldspar	8	12	7	8	7
Potassium Feldspar	6	4	4	8	4
Calcite ($CaCO_3$)	nd	nd	nd	nd	nd
Dolomite ($CaMg[CO_3]_2$)	*trace*	*trace*	*trace*	*trace*	1
Siderite ($FeCO_3$)	nd	*trace*	nd	nd	nd
Pyrite (FeS_2)	nd	nd	nd	nd	nd
Mica and/or Illite	2	2	1	2	8
Kaolinite	5	4	3	2	3
Chlorite	*trace*	*trace*	*trace*	*trace*	*trace*
Mixed-Layer Illite (%)/Smectite	2 (40)	9 (80)	6 (80)	7 (60)	1 (60)
TOTALS	100%	100%	100%	100%	100%

Mineral Phases	Lower Hemlock				
	6	7	15	8	9
	14801.8	**14848.2**	**14877.3**	**14905'**	**14924.3**
Quartz (SiO_2)	65	69	31	74	78
Plagioclase Feldspar	12	5	3	9	6
Potassium Feldspar	5	5	1	3	3
Calcite ($CaCO_3$)	nd	11	nd	nd	nd
Dolomite ($CaMg[CO_3]_2$)	*trace*	*trace*	*trace*	*trace*	*trace*
Siderite ($FeCO_3$)	nd	nd	1	nd	nd
Pyrite (FeS_2)	nd	nd	nd	nd	nd
Mica and/or Illite	6	1	10	1	7
Kaolinite	5	3	18	4	3
Chlorite	*trace*	*trace*	2	*trace*	*trace*
Mixed-Layer Illite (%)/Smectite	5 (80)	5 (50)	33 (60)	8 (70)	2 (70)
TOTALS	100%	100%	100%	100%	100%

Review of the air-dried and glycol-solvated clay slides indicates that these mixed-layer illite/smectite clays are composed of approximately 30%- 70% expandable smectite layers.

nd - if present, the amount was below the detectable capabilities of x-ray diffraction analysis.

Table #3 (continued) - Mineralogical Analysis (in Weight Percents)

Mineral Phases	Lower Hemlock				
	10	11	12	13	14
	14925.0	**14940'**	**14940.3**	**15002.7**	**15025.7**
Quartz (SiO_2)	82	41	78	69	77
Plagioclase Feldspar	6	19	7	10	6
Potassium Feldspar	2	16	3	6	5
Calcite ($CaCO_3$)	nd	nd	nd	nd	nd
Dolomite ($CaMg[CO_3]_2$)	1	1	*trace*	*trace*	*trace*
Siderite ($FeCO_3$)	*trace*	*trace*	nd	nd	nd
Pyrite (FeS_2)	nd	*trace*	nd	nd	nd
Mica and/or Illite	1	3	5	3	1
Kaolinite	4	7	3	5	3
Chlorite	*trace*	*trace*	*trace*	1	*trace*
Mixed-Layer Illite (%)/Smectite	3 (80)	11 (80)	3 (80)	5 (30)	7 (60)
TOTALS	100%	100%	100%	100%	100%

Review of the air-dried and glycol-solvated clay slides indicates that these mixed-layer illite/smectite clays are composed of approximately 30%- 70% expandable smectite layers.

nd - if present, the amount was below the detectable capabilities of x-ray diffraction analysis.

Figure #1 - Mineralogical Analysis (XRD Results in Weight Percents)

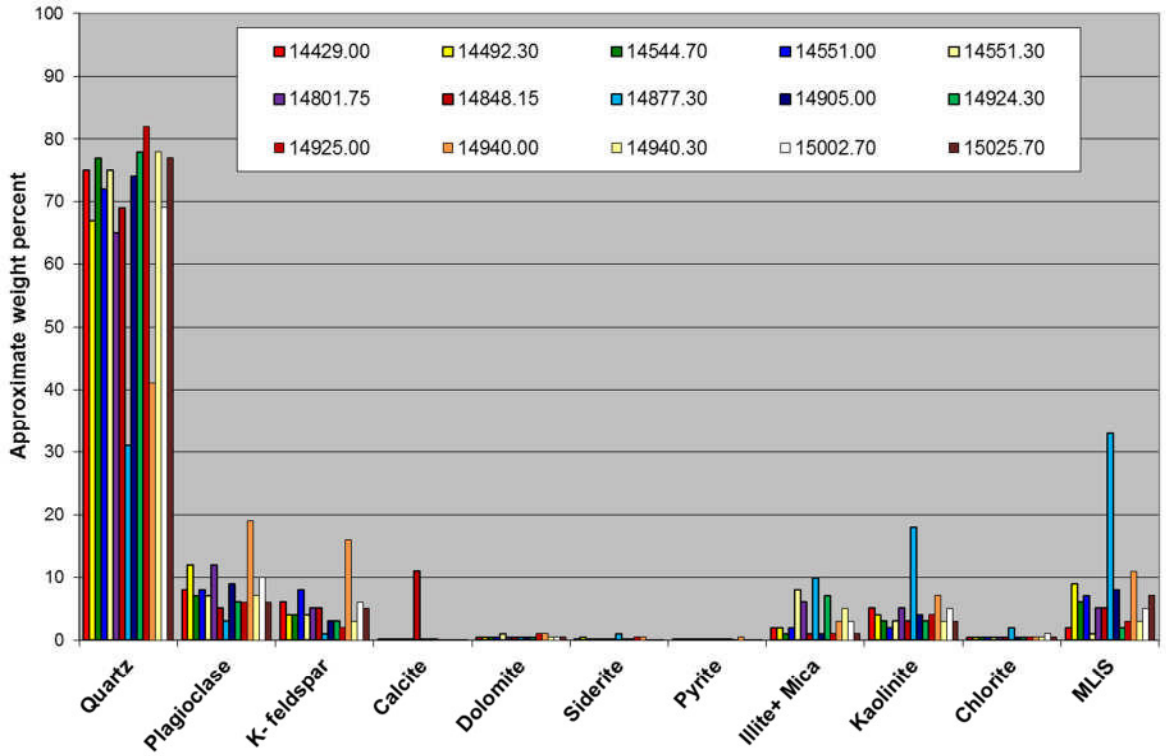

Capillary Suction Time Testing (CST)

CST testing defines the time of movement of a water front between two electrodes, which is related to the ability of the fluid to flocculate or disperse clays in a sample. CST results are presented as capillary suction time ratios. The selected liquids are tested without solids to create a baseline for comparison to sample+liquid travel times. CST ratios are defined as the sample+liquid travel time divided by the corresponding liquid-only travel time. When comparing multiple samples in the same fluid, the longer the time of water front movement, the greater the water sensitivity of the sample (the greater the dispersion). When comparing the same sample in different fluids, the higher CST ratios indicate poorer clay control by the fluid. CST analysis homogenizes rock samples, therefore exposing all clays or other reactive minerals with the testing solution. This is not a completely valid simulation of the downhole reservoir, since any clay within shale laminations or shale clasts will be exposed to treatment fluids. Additionally, CST analysis is influenced by fluid pH and formation grainsize, which can cause misinterpretation of data. CST analysis therefore tends to overestimate the sensitivity of formations to treatment fluids, but can be used as a comparator to get a better feel for sensitivity to treatment solutions given the limitations of the analytical procedure.

CST testing was performed on cored material to evaluate these zone's reaction to two fluids: tapwater and 3% KCl. To date, the data indicates a relatively low sensitivity to low salinity brines other than the clay-rich mudstone.

Figure #2 – Capillary Suction Time Testing Results

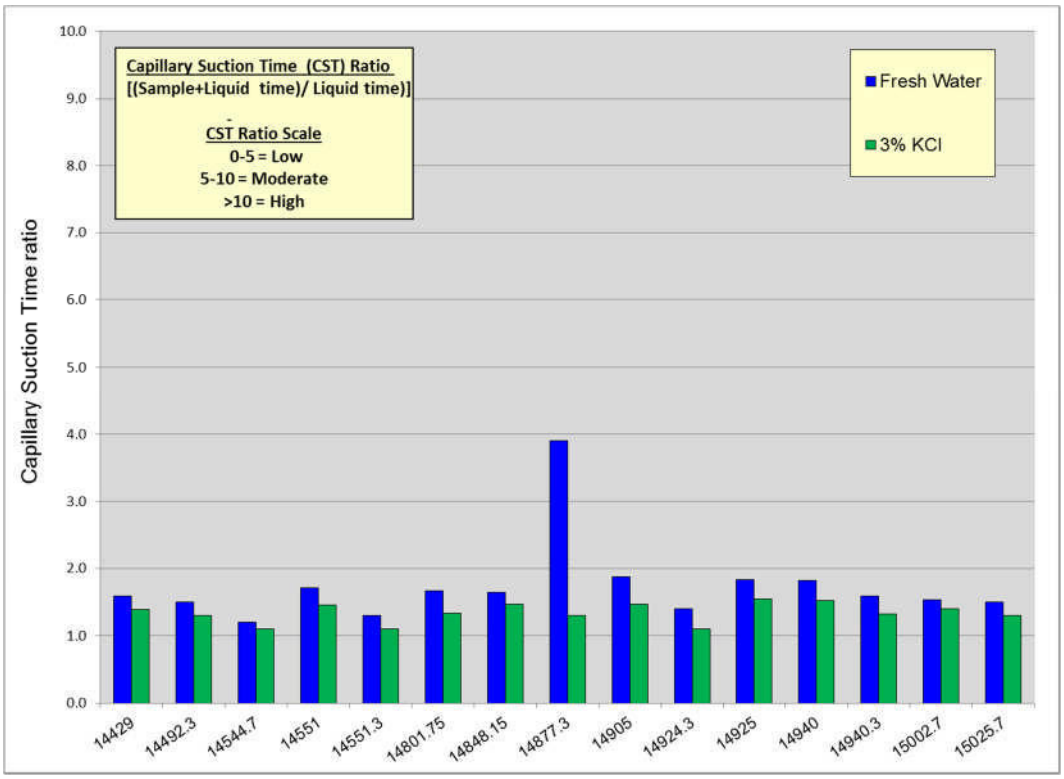

Scanning Electron Microscopy

Formation chips were cleaned with hydrocarbon solvents and dried in a convection oven. Fresh surfaces were obtained by cracking the chips open; these pieces were subsequently mounted on aluminum sample holders for SEM/EDS analysis. The attached SEM photoplates

document the rock/pore network seen in these samples, and illustrate specific examples of common features at varying magnifications.

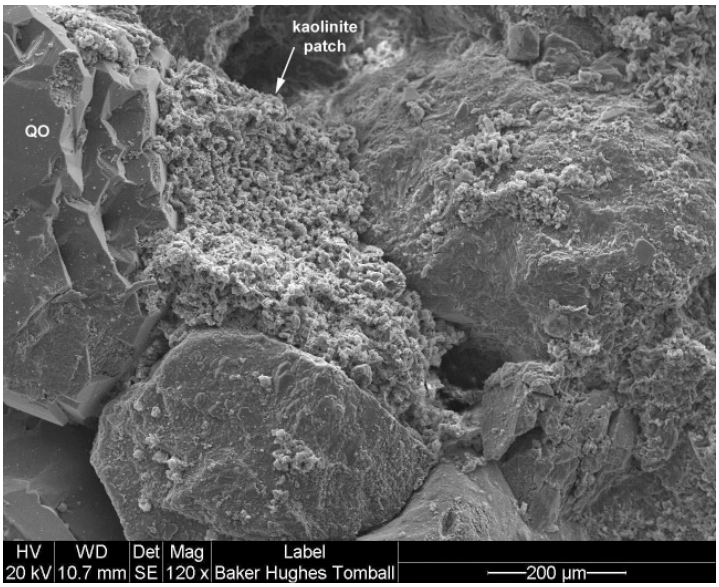

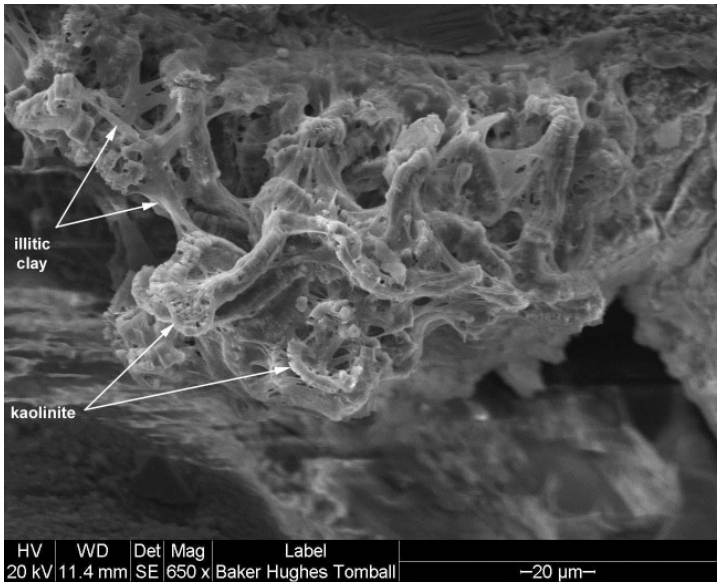

These samples were predominantly pebble conglomerates that contained a mixture of pebbles, granules, sand, silt, and clay. Sorting therefore was generally poor, excepting two of the well-sorted sandstone samples (14492.3' & 15002.7'). Intergranular cementation was primarily by a mix of detrital and authigenic clays, and overburden compaction. Lesser amounts of authigenic cements were noted, including quartz overgrowths and calcite. The combination of authigenic clays, authigenic cements, and overburden compaction has reduced intergranular porosity from the original detrital levels. Most of the samples exhibited Fair or Fair to Poor levels of intergranular porosity. Secondary porosity created by the partial dissolution of feldspars slightly increases the total porosity, but most of the secondary porosity appears to be micropores inside the degraded feldspar grains. Microporosity associated with the detrital and authigenic clays is abundant in almost all samples, and appears to be the dominant porosity type in the clay-rich samples at the top of the Lower Hemlock unit (14801-14848').

Kaolinite, chlorite, illite, and mixed-layer illite/smectite were noted in the mineralogical analysis, and were observed in a variety of morphologies in these samples. Classic kaolinite pseudohexagonal booklets were noted frequently in large pore-filling patches that have a significant negative impact on permeability. The 120X view from 14429' shows a typical example of the kaolinite patches, that fill pre-existing pores. Kaolinite was also noted as a pore-filling precipitate in vermicular forms that did not appear to have distinct platelets (see Photoplate 2B and image at right). Blocky detrital forms of chlorite and illitic clays were noted as intergranular cement, which also lines intergranular pores. Grain-parallel illite coats framework grains, and appears to be commonly recrystallized. Filamentous forms of illite, commonly referred to as "hairy" illite were noted on kaolinite patch surfaces, and in pore-bridging structures. Sheet-like flakes of **illitic** clays with wispy, fibrous terminations were noted growing from grain-coating forms, into and across pores and pore-throats.

PHOTOPLATES

PHOTOPLATE 1 - SCANNING ELECTRON MICROSCOPE PHOTOMICROGRAPHS
Upper Hemlock Formation - 14429.0 ft.

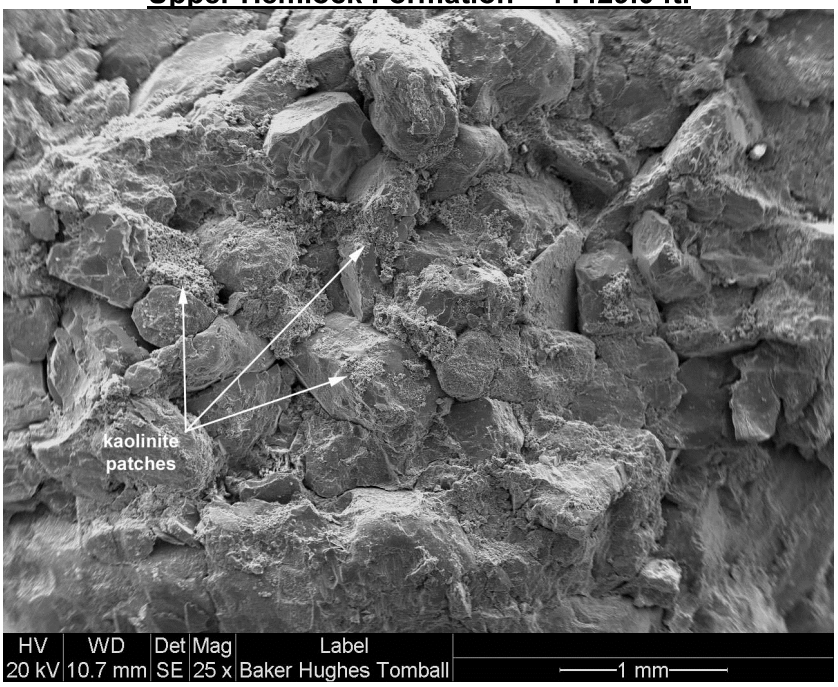

VIEW A : Detrital grains are seen cemented by clays, quartz overgrowths, and overburden compaction. Intergranular porosity is described as Fair, but microporosity is extensive.

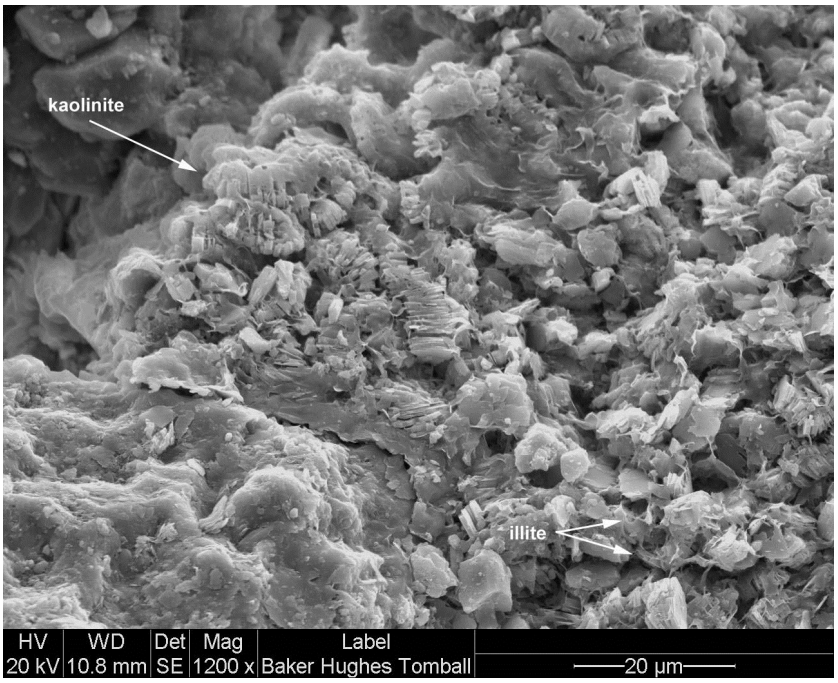

VIEW B : Patches of pore-filling kaolinite booklets are common in this pebble conglomerate, with wispy forms of illite intermixed with the kaolinite.

PHOTOPLATE 2 - SCANNING ELECTRON MICROSCOPE PHOTOMICROGRAPHS

Upper Hemlock Formation - 14492.3 ft.

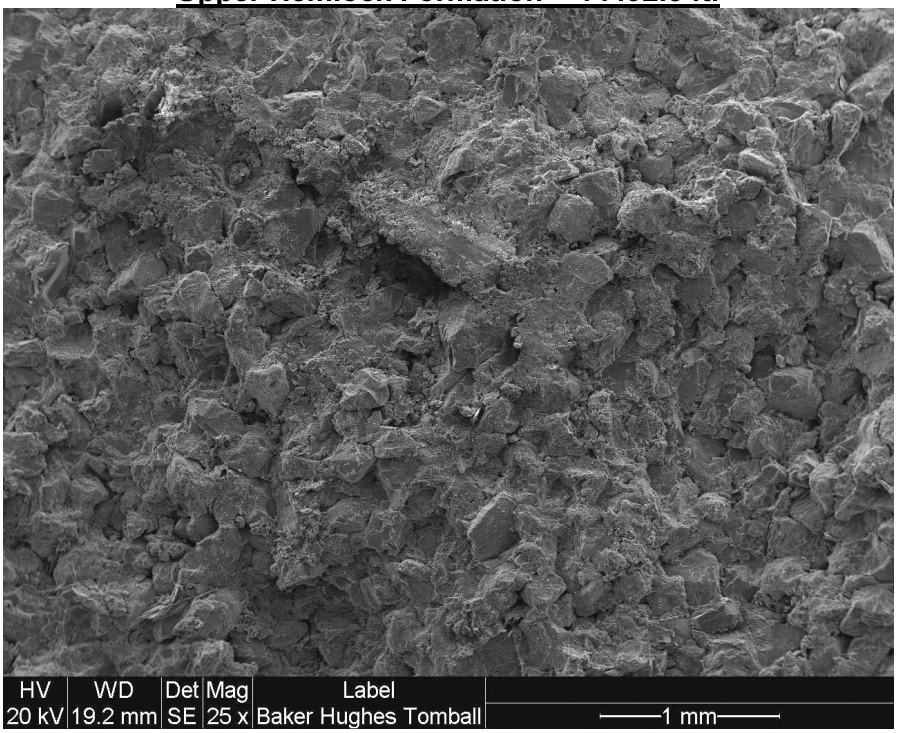

VIEW A : This well-sorted sandstone is cemented by clays and compaction, which combined with the smaller grain size have reduced poro/perm values to moderate levels.

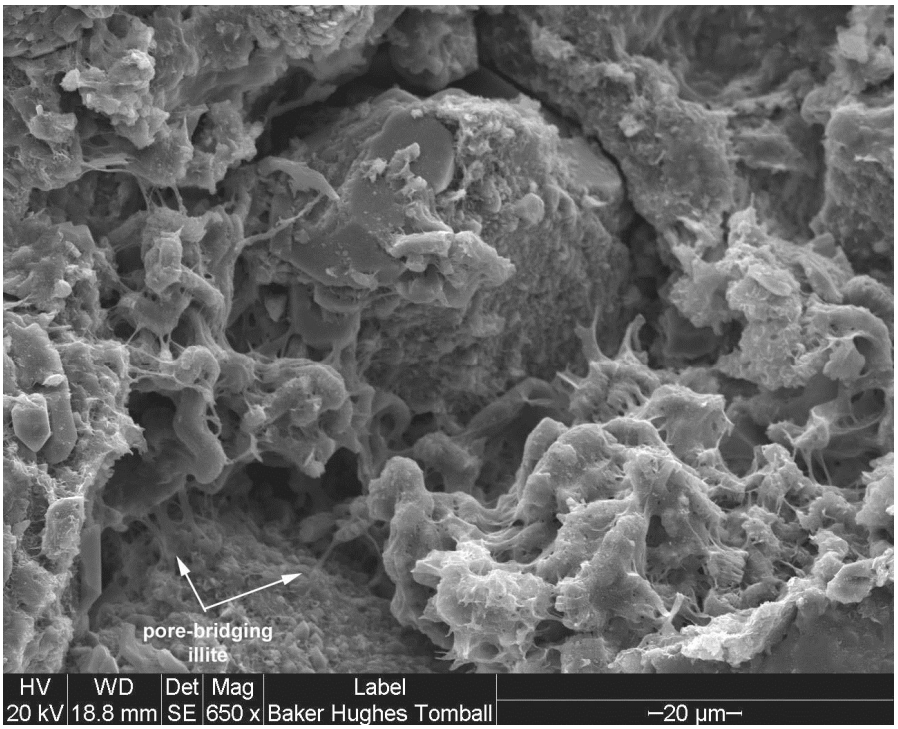

VIEW B : Oddly-shaped, semi-vermicular kaolinite is visible above, along with filamentous forms of illite precipitated later in diagenesis.

PHOTOPLATE 3 - SCANNING ELECTRON MICROSCOPE PHOTOMICROGRAPHS
Upper Hemlock Formation - 14544.7 ft.

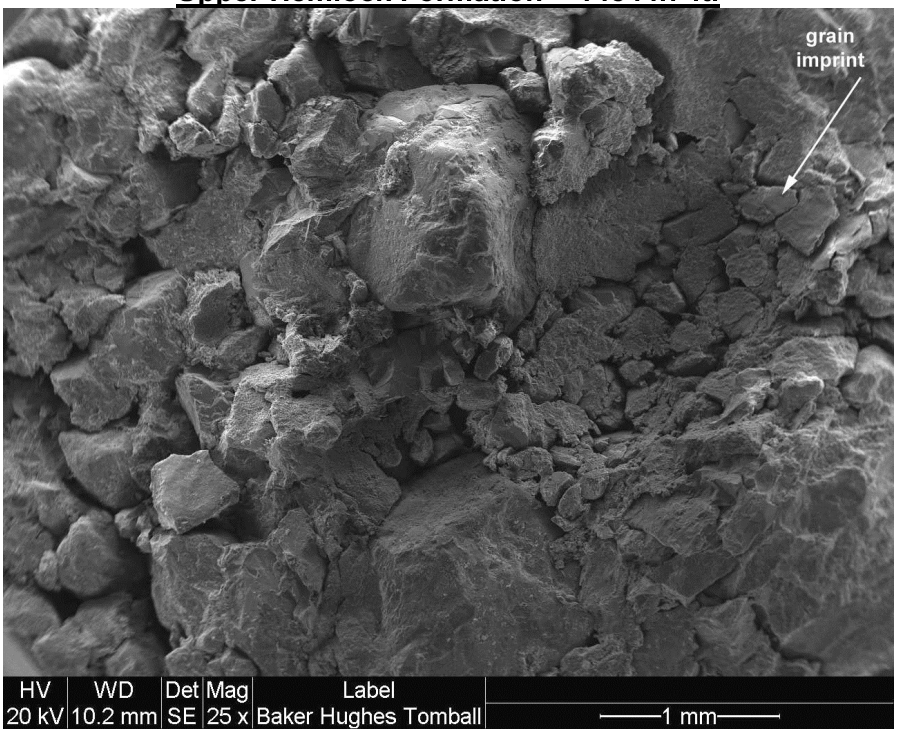

VIEW A : Detrital grains are seen cemented by clays and overburden compaction. Intergranular pores are clearly visible in the grain imprint at right-center.

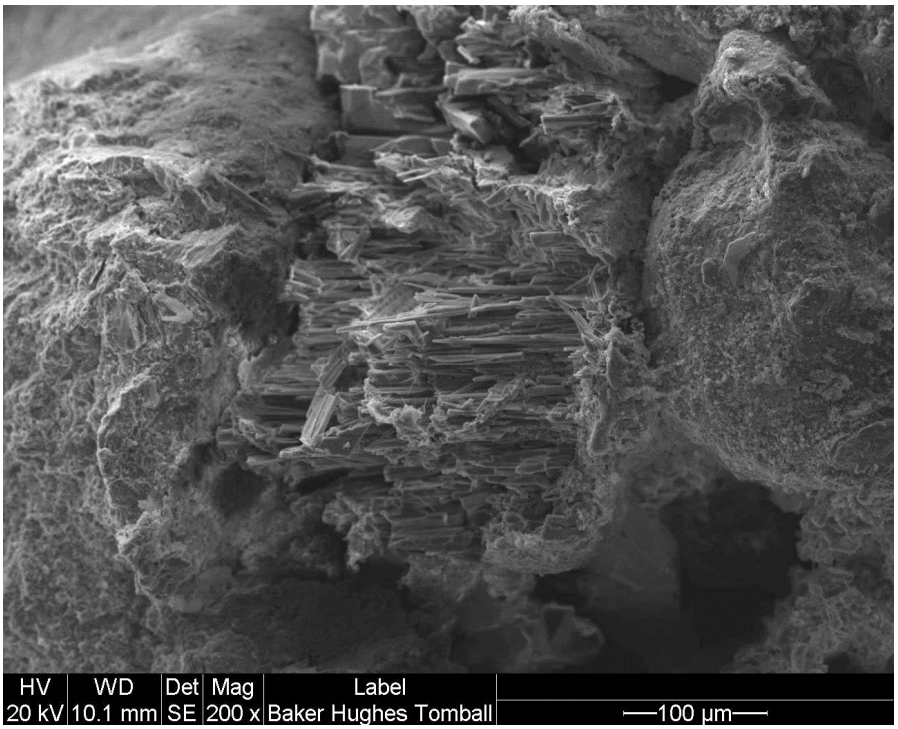

VIEW B : Microporosity is visible within this degraded feldspar, but microporosity is minor at this depth relative to the abundant intergranular porosity.

PHOTOPLATE 4 - SCANNING ELECTRON MICROSCOPE PHOTOMICROGRAPHS

Upper Hemlock Formation - 14551.0 ft.

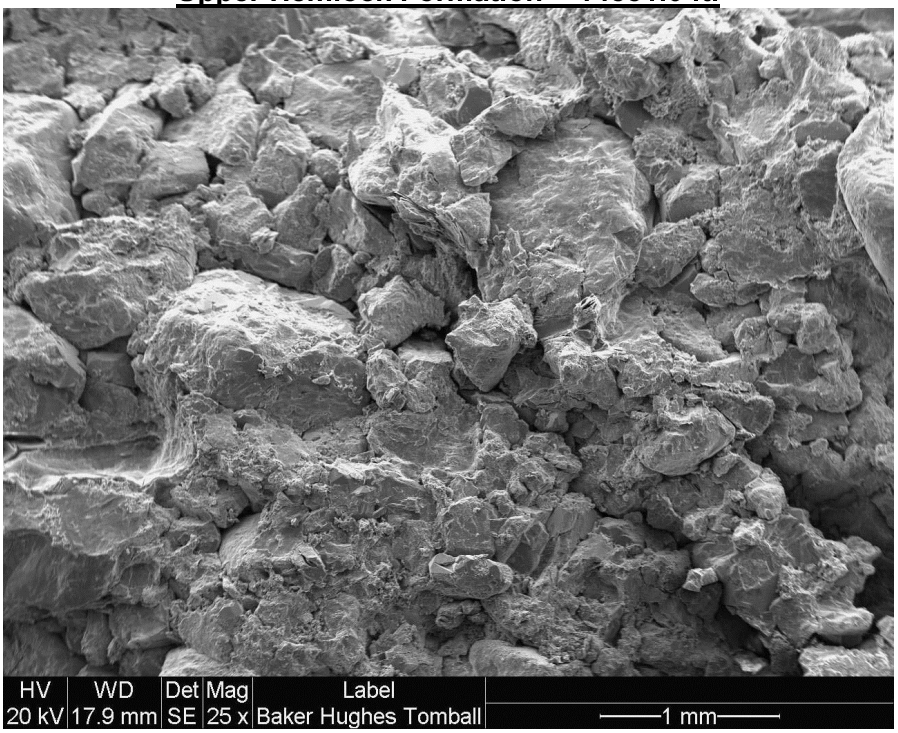

VIEW A : This conglomeritic sandstone exhibits Fair intergranular porosity, with triangular-shaped pores common between grains. Clay-assocated microporosity is only present in moderate amounts.

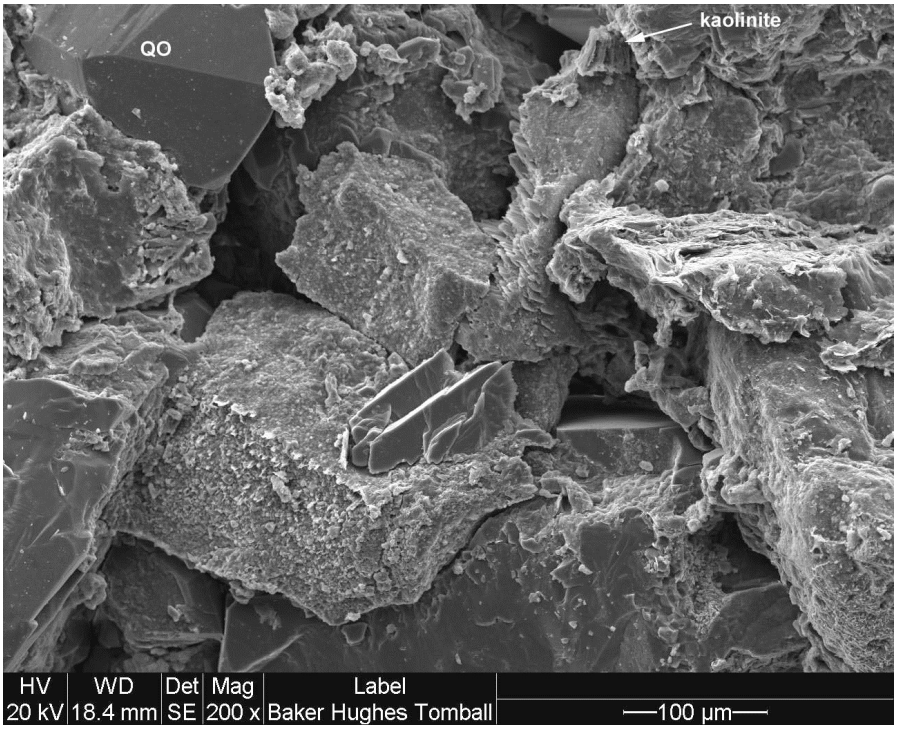

VIEW B : Decreased amounts of clays and quartz overgrowths result in better reservoir quality in this sample. Note the open pore-throats above.

PHOTOPLATE 5 - SCANNING ELECTRON MICROSCOPE PHOTOMICROGRAPHS
Upper Hemlock Formation - 14551.3 ft.

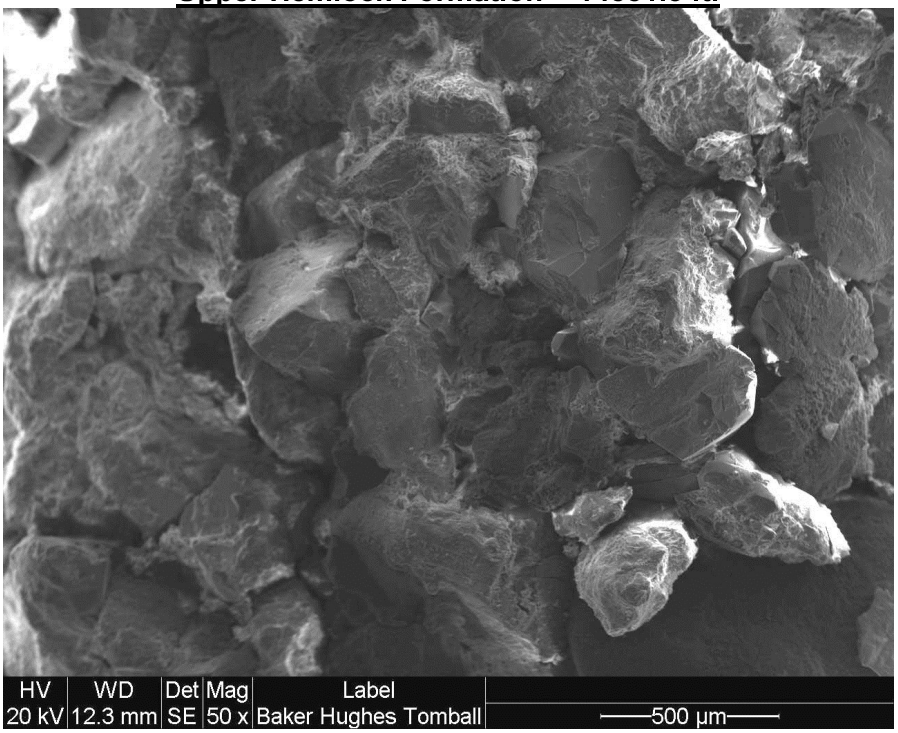

VIEW A :

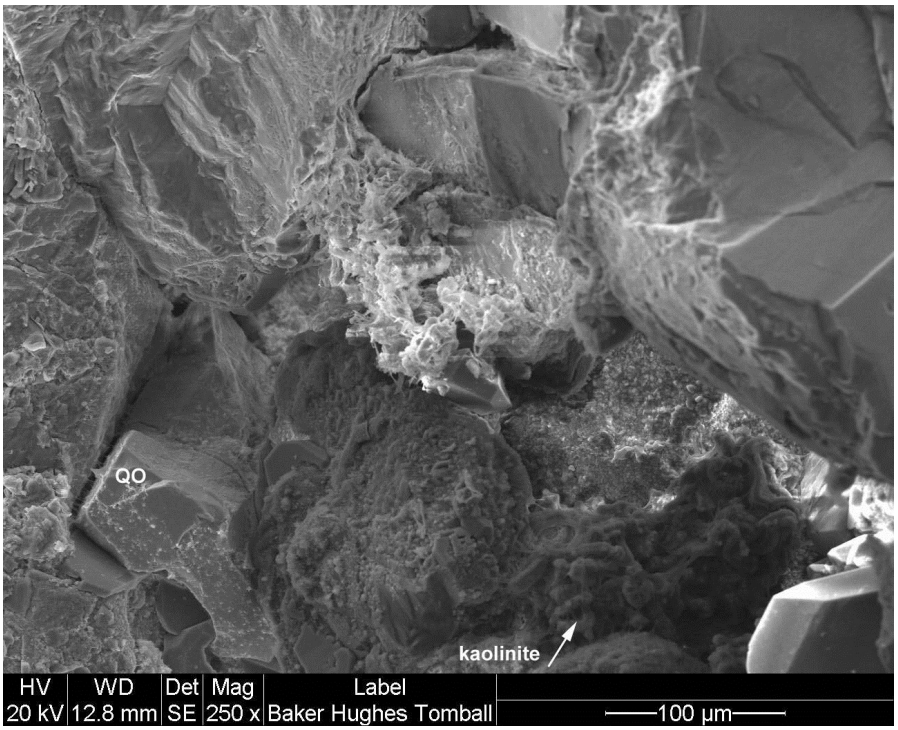

VIEW B :

PHOTOPLATE 6 - SCANNING ELECTRON MICROSCOPE PHOTOMICROGRAPHS

Lower Hemlock Formation - 14801.8 ft.

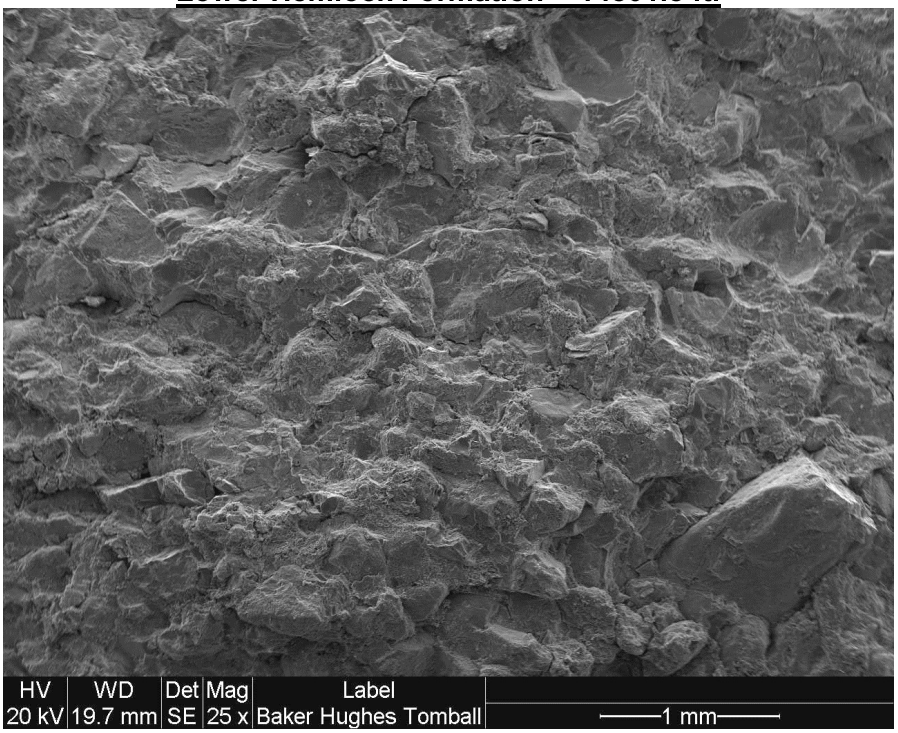

VIEW A : This sample is well-cemented by clays and compaction, reducing intergranular porosity to Poor levels.

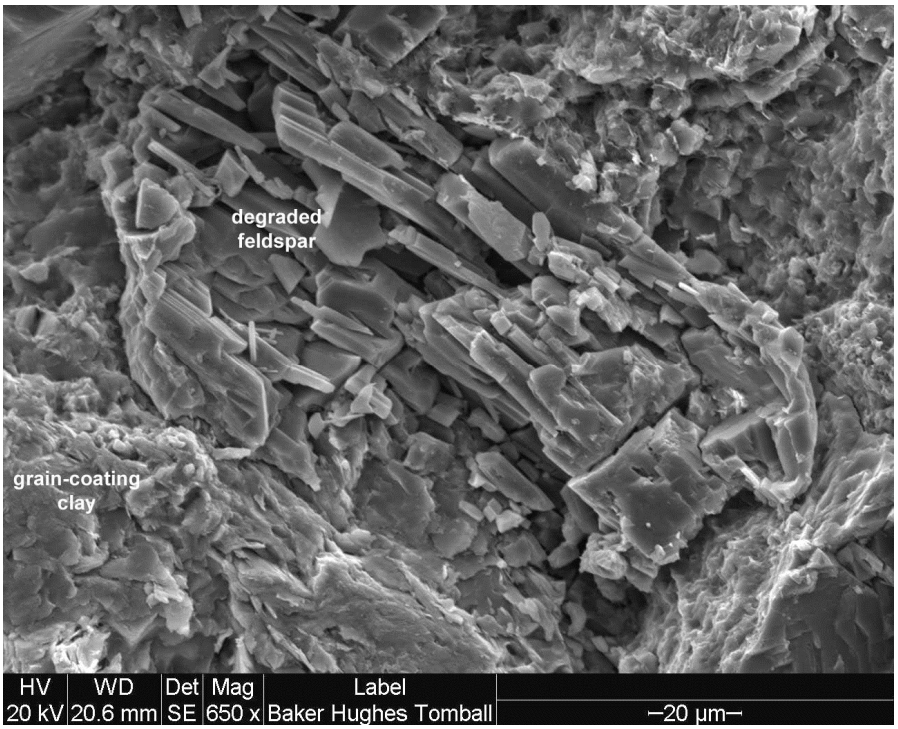

VIEW B : The interior of this feldspar indicates that it has undergone partial dissolution and recrystallization along the cleavage planes. Note the microporosity inside the grain. Blocky forms of grain-coating clays are visible at bottom-left and upper-right.

PHOTOPLATE 7 - SCANNING ELECTRON MICROSCOPE PHOTOMICROGRAPHS
Lower Hemlock Formation - 14848.2 ft.

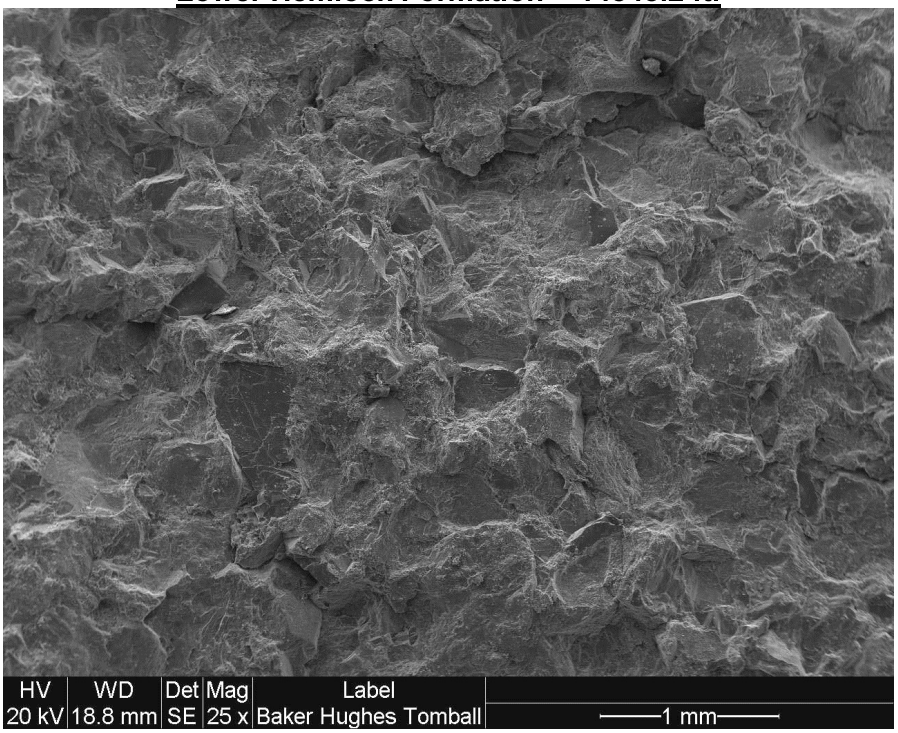

VIEW A : This sample is heavily-cemented by clays, compaction, and calcite, which have reduced intergranular porosity to Poor levels. Microporosity associated with the clays is the dominant porosity type, and is extensive.

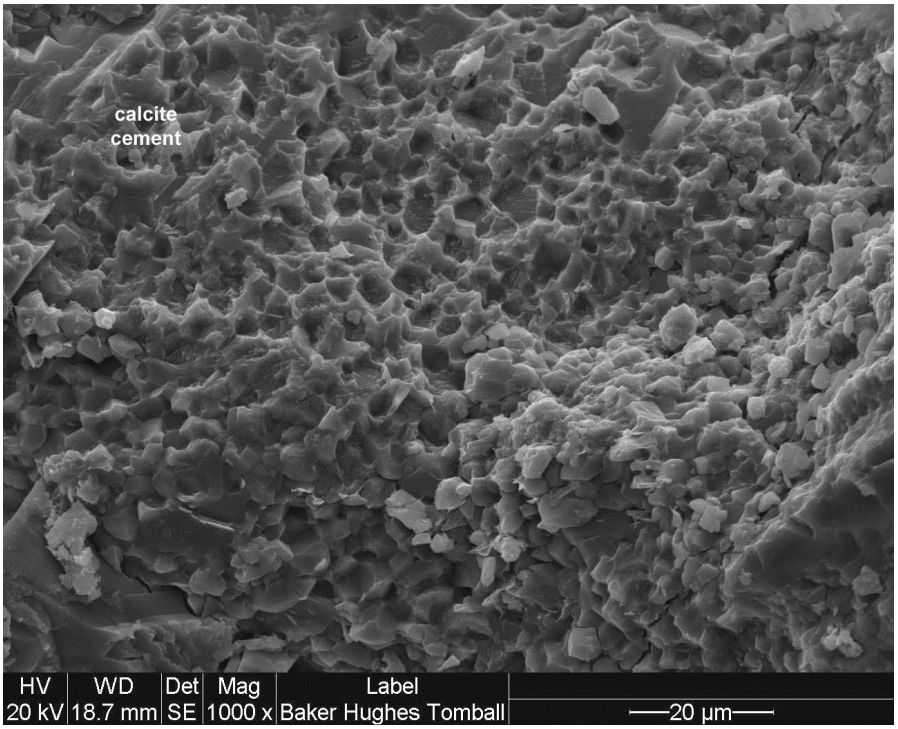

VIEW B : This view shows imprints of kaolinite in a calcite cement, confirming multiple cycles of authigenic precipitation.

PHOTOPLATE 8 - SCANNING ELECTRON MICROSCOPE PHOTOMICROGRAPHS
Lower Hemlock Formation - 14905.0 ft.

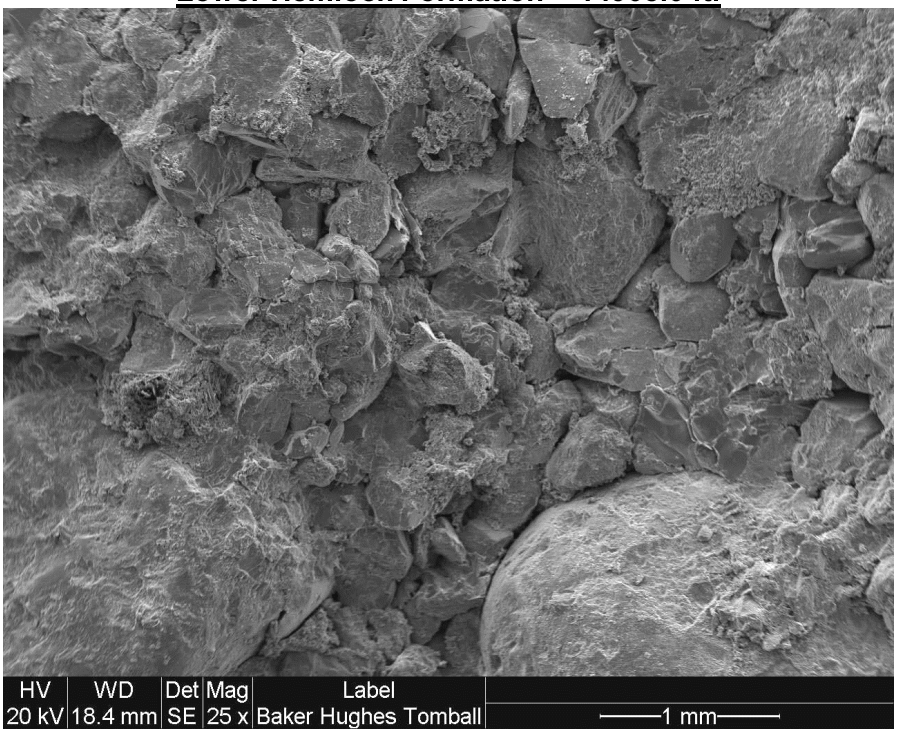

VIEW A : This pebble conglomerate exhibits Fair intergranular porosity, but microporosity associated with the clay cement is extensive.

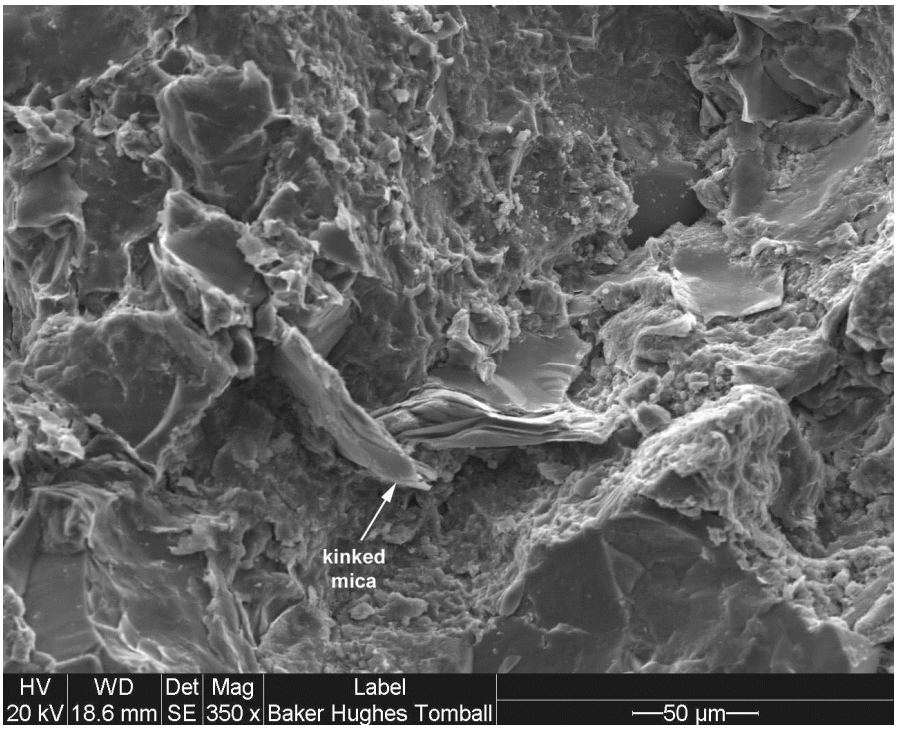

VIEW B : Quartz, feldspar, and mica grains are cemented by clays and compaction. Pore-filling kaolinite is the primary authigenic porosity reducer.

PHOTOPLATE 9 - SCANNING ELECTRON MICROSCOPE PHOTOMICROGRAPHS
Lower Hemlock Formation - 14924.3 ft.

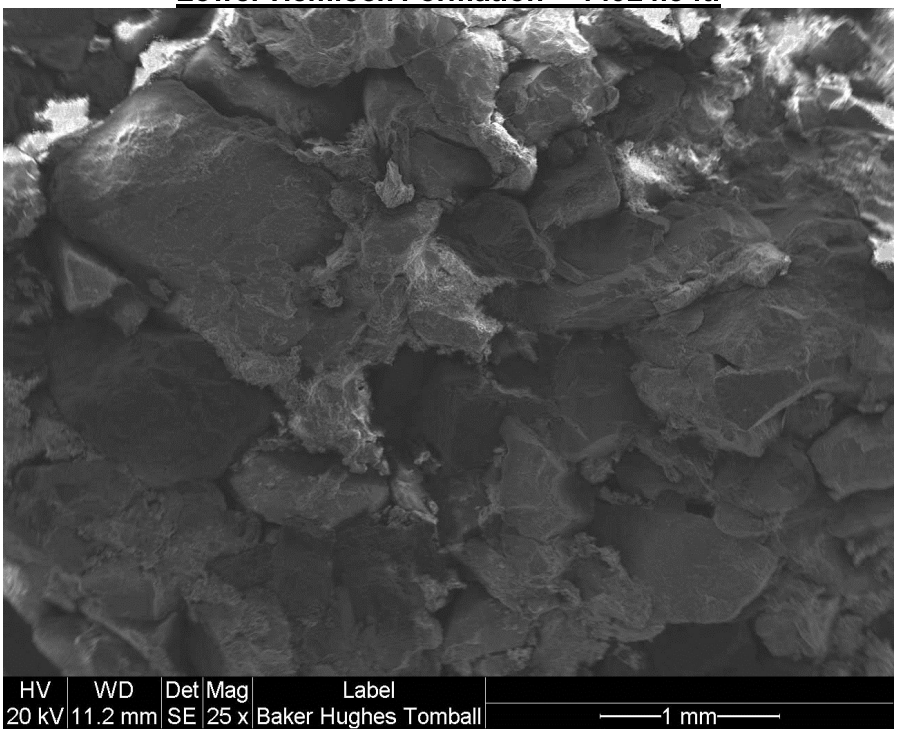

VIEW A : Detrital grains are cemented by clays, compaction, and lesser amounts of quartz overgrowths.

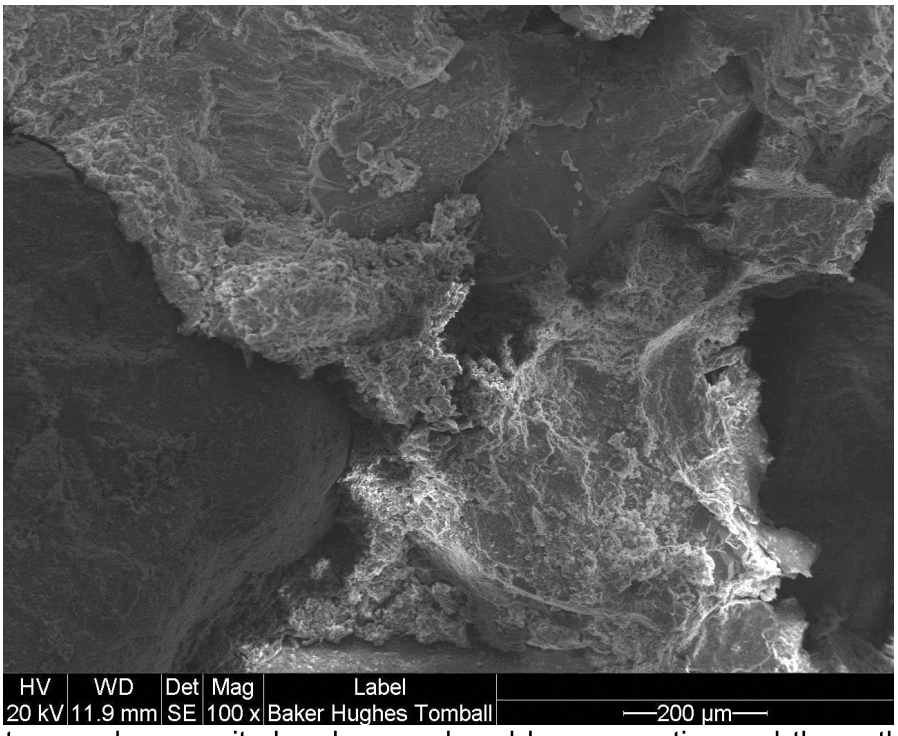

VIEW B : Intergranular porosity has been reduced by compaction and the authigenic pore-filling clays visible above.

PHOTOPLATE 10 - SCANNING ELECTRON MICROSCOPE PHOTOMICROGRAPHS
Lower Hemlock Formation - 14925.0 ft.

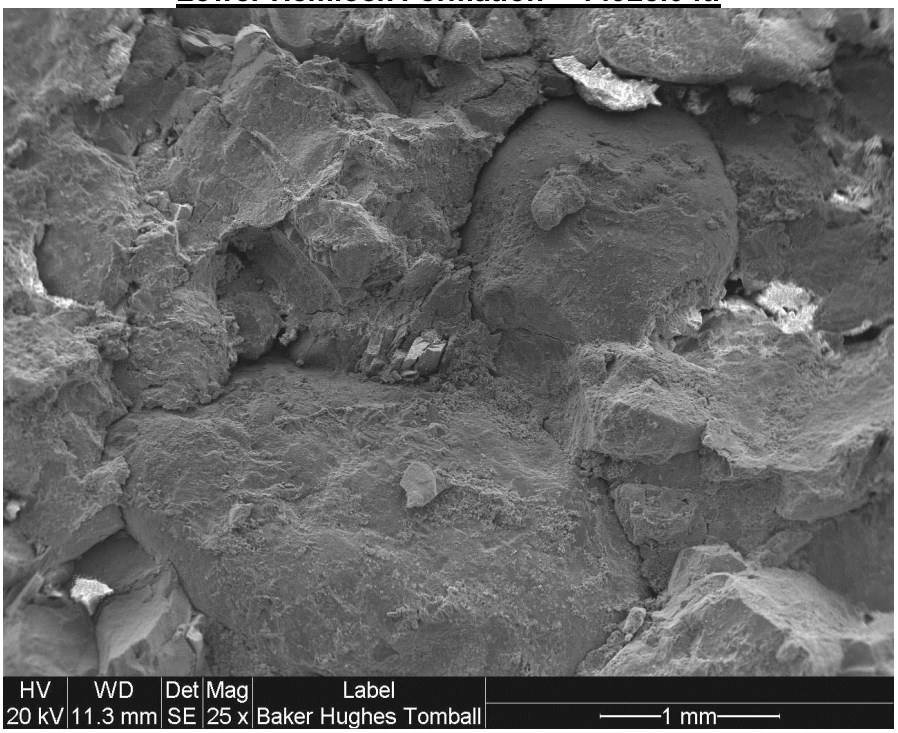

VIEW A : Intergranular porosity is described as Fair to Good. Clays and compaction are the primary cement; traces of quartz overgrowths are present. Small amounts of authigenic dolomite microcrystals were also noted.

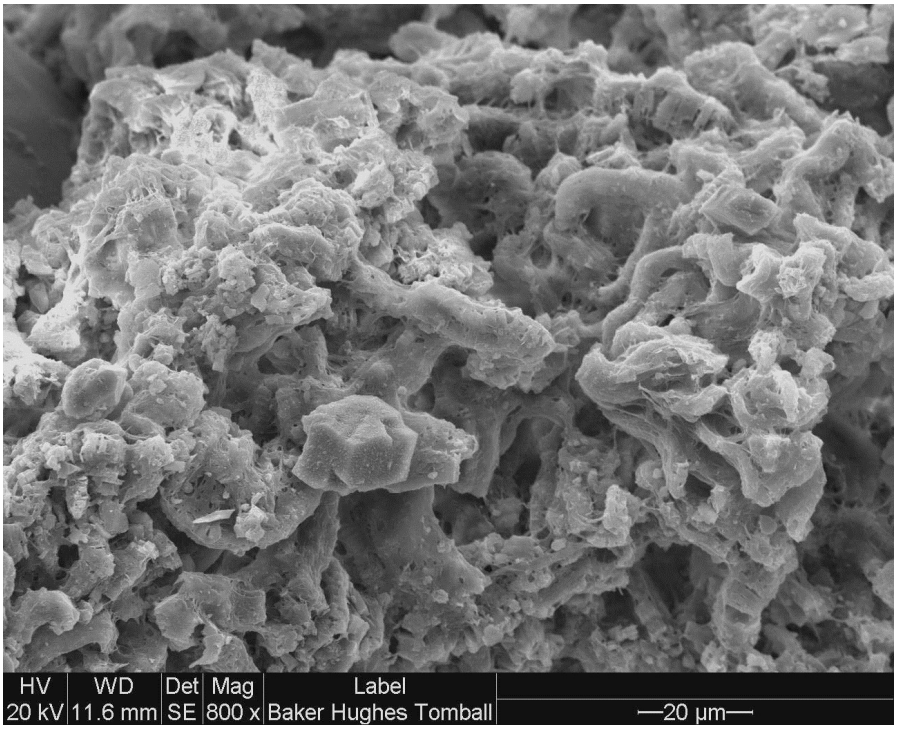

VIEW B : Semi-vermicular forms of kaolinite form pore-filling masses in this pebble conglomerate. Filamentous illite is visible on the kaolinite surfaces.

PHOTOPLATE 11 - SCANNING ELECTRON MICROSCOPE PHOTOMICROGRAPHS
Lower Hemlock Formation - 14940.0 ft.

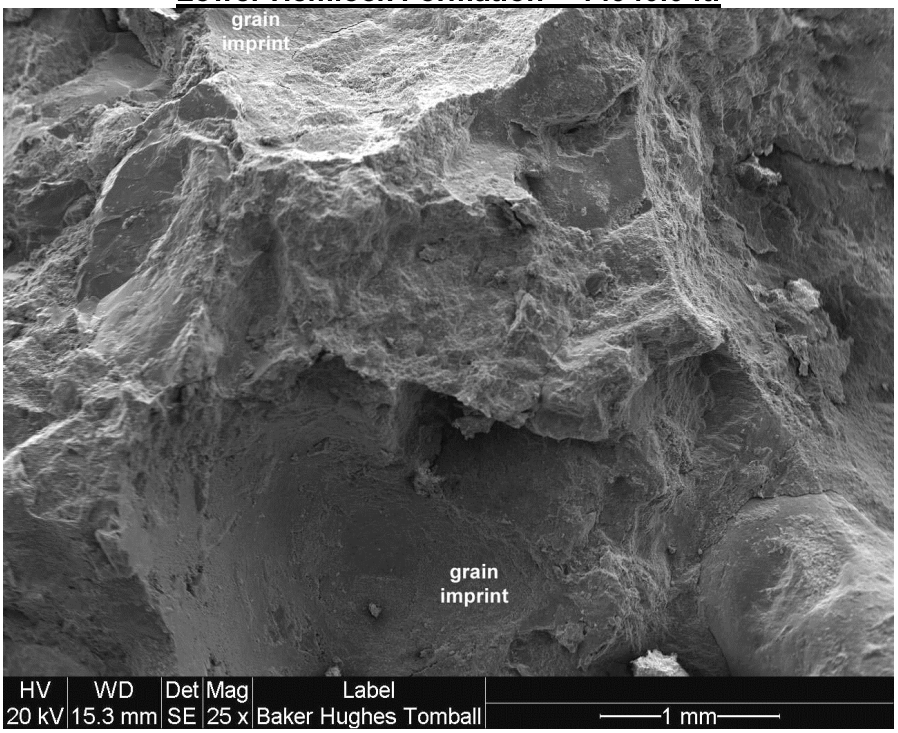

VIEW A : Very large pebbles form inprints in clay at top, bottom, and far right. Clays and compaction are the dominant cements. Intergranular porosity is described as Poor due to the abundant clay matrix cement.

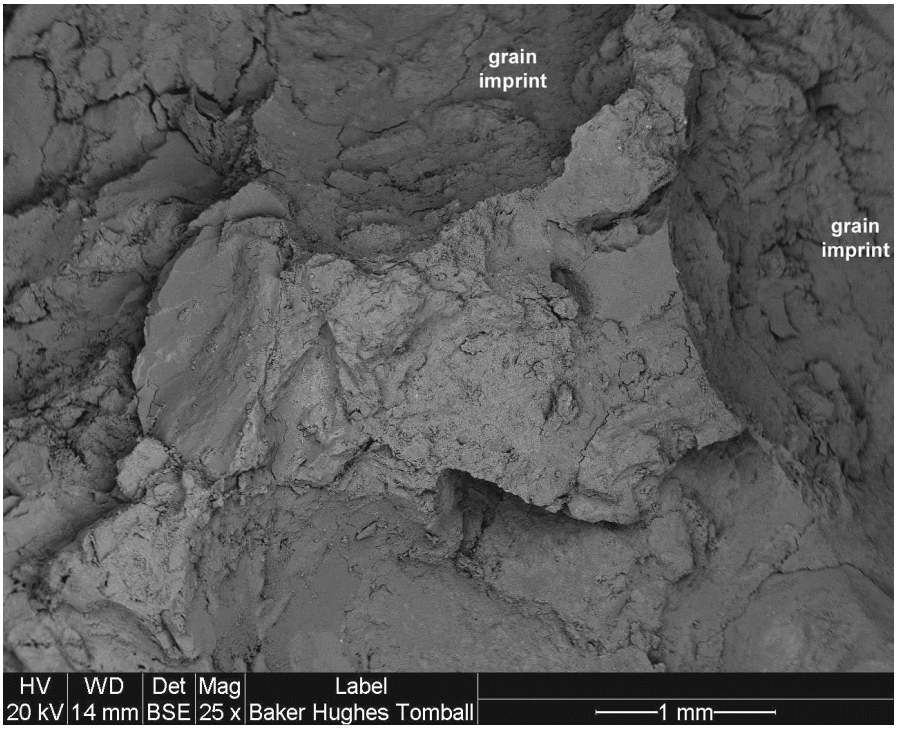

VIEW B : Backscattered electron detector view of the image above. EDS elemental analysis indicates that the clay cement at center is dominantly chlorite.

PHOTOPLATE 12 - SCANNING ELECTRON MICROSCOPE PHOTOMICROGRAPHS
Lower Hemlock Formation - 14940.3 ft.

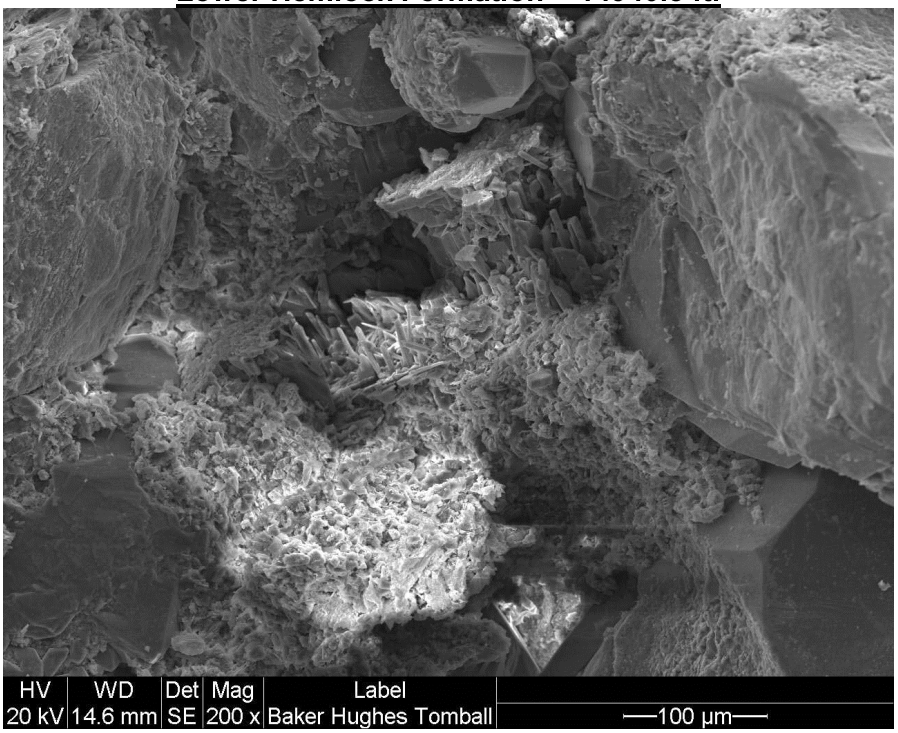

VIEW A : A partially-degraded feldspar is seen at center; pore-filling kaolinite is visible at lower-center.

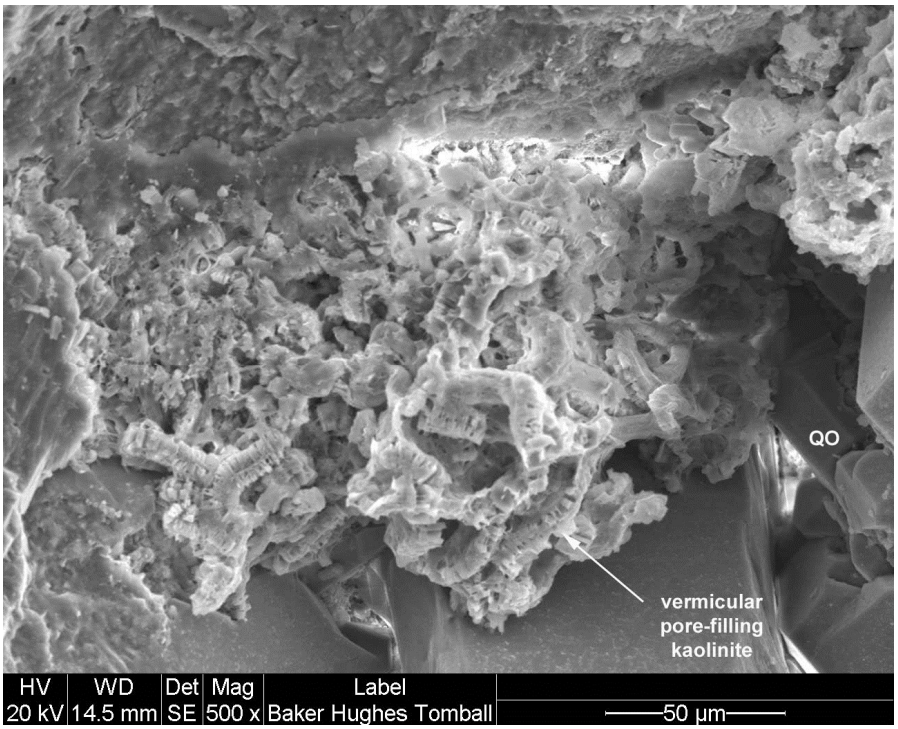

VIEW B : Vermicular kaolinite containing abundant microporosity is visible above.

PHOTOPLATE 13 - SCANNING ELECTRON MICROSCOPE PHOTOMICROGRAPHS
Lower Hemlock Formation - 15002.7 ft.

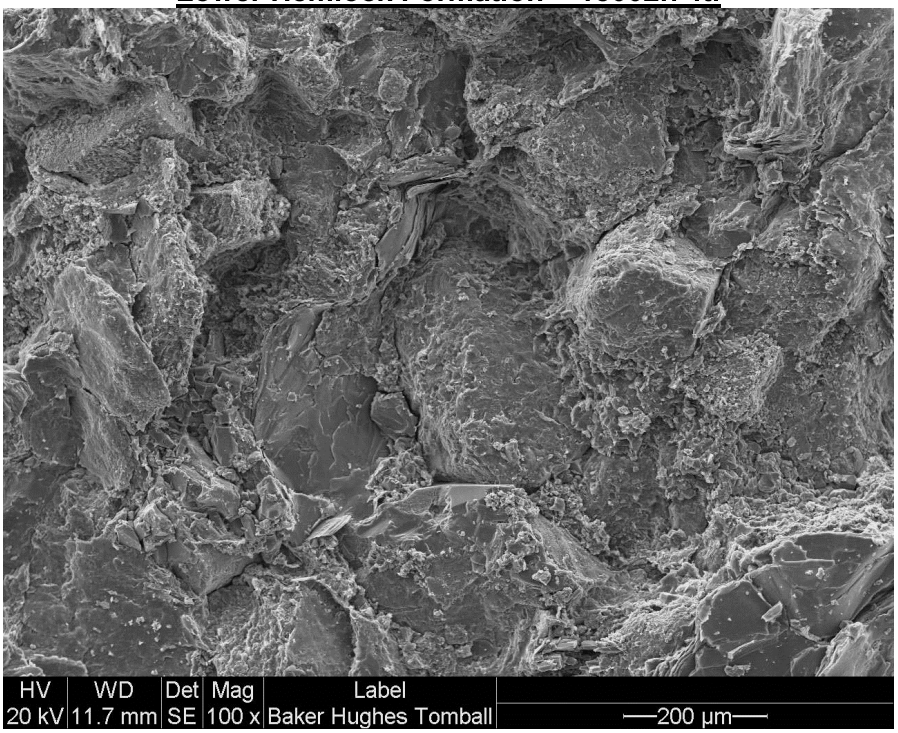

VIEW A : Intergranular porosity of this fine-grained sandstone is Fair, but the clay and overburden compaction reduce the average size of the pore throats, decreasing permeability. A kinked mica grain is seen at upper-center.

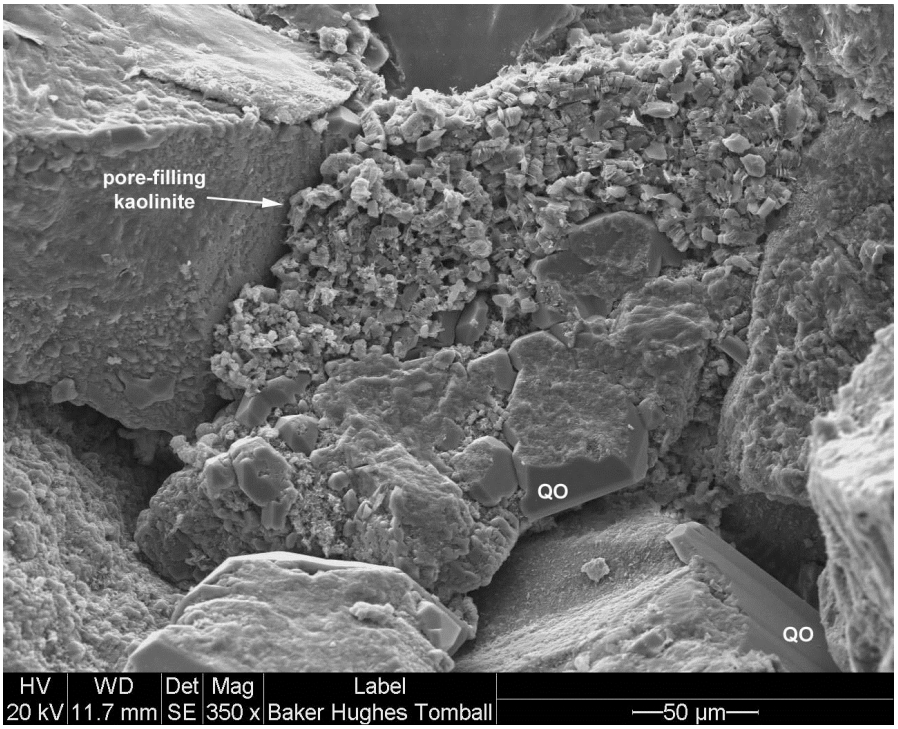

VIEW B : Kaolinite booklets are visible filling an intergranular pore, increasing the cementation of the sample. Incipient quartz overgrowths are seen at center.

PHOTOPLATE 14 - SCANNING ELECTRON MICROSCOPE PHOTOMICROGRAPHS
Lower Hemlock Formation - 15025.7 ft.

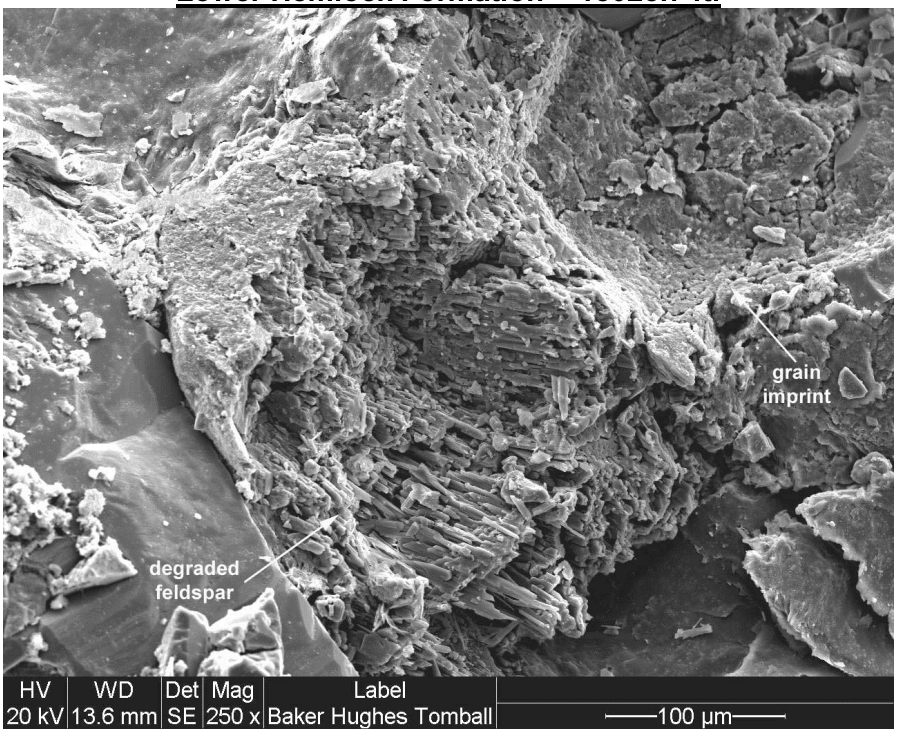

VIEW A : Microporosity inside a partially-degraded feldspar is visible at center and top-center.

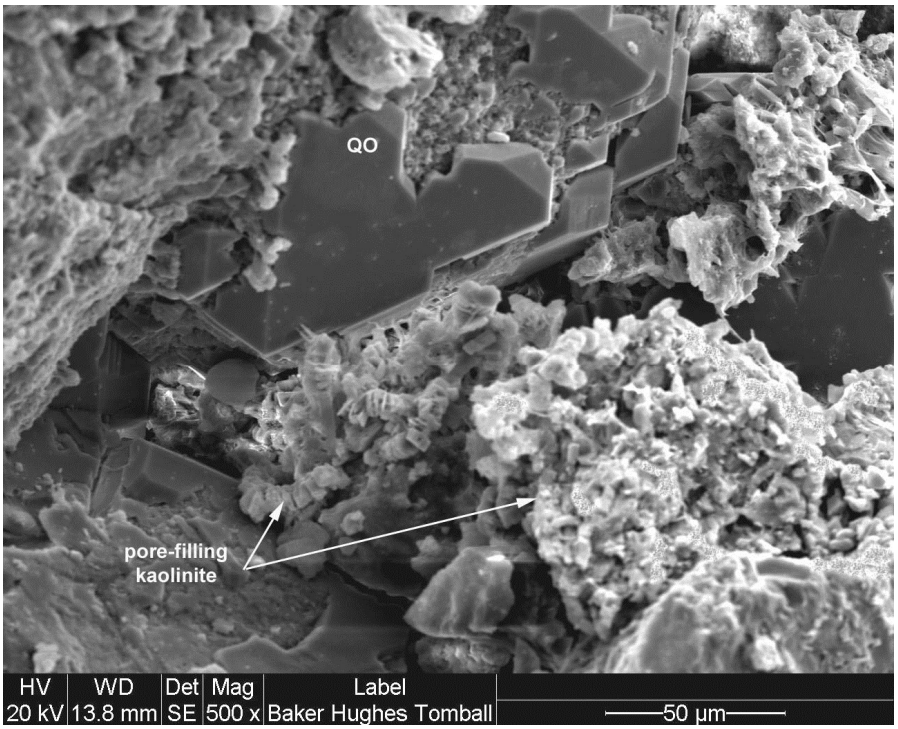

VIEW B : Porosity reduction by authigenic minerals is evident by the quartz overgrowths and pore-filling kaolinite mass.

PHOTOPLATE 15 - SCANNING ELECTRON MICROSCOPE PHOTOMICROGRAPHS
Lower Hemlock Formation - ?14877.3 ft.

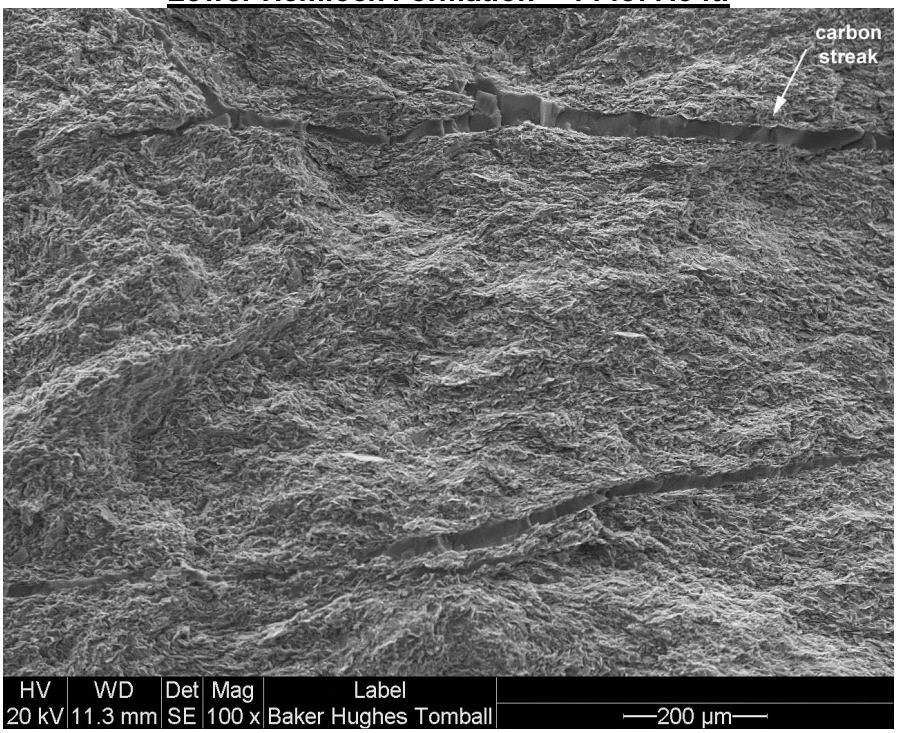

VIEW A : This mudstone sample contained small carbonaceous streaks probably associated with detrital plant matter.

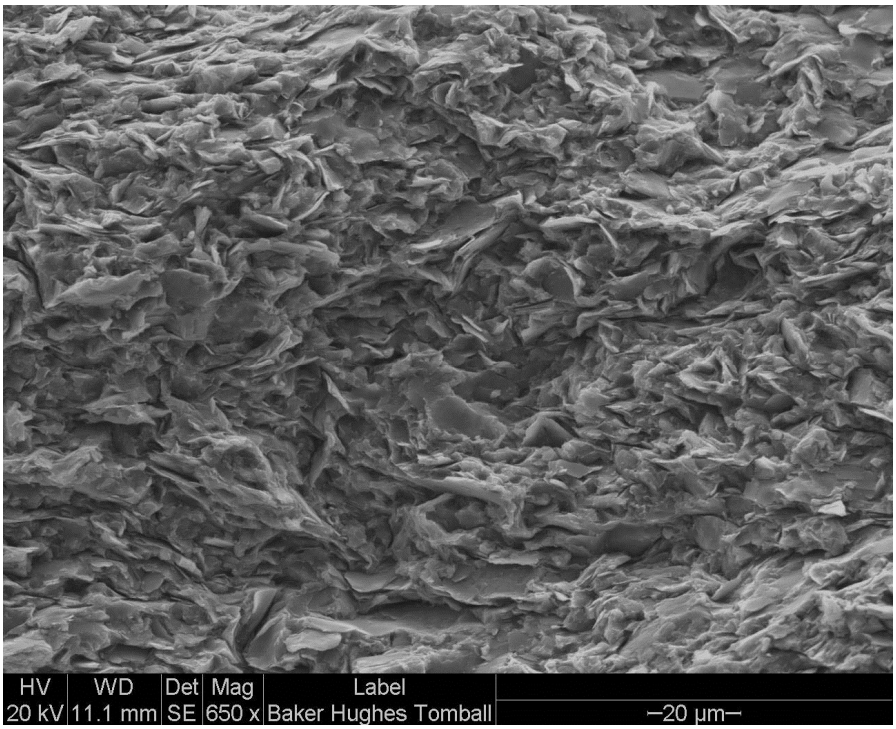

VIEW B : The clay-sized fabric is tightly interwoven and compacted by overburden forces, limiting intergranular porosity.

ANALYTICAL PROCEDURES

Scanning Electron Microscopy/Energy Dispersive Spectrometry

Scanning electron microscopy/energy dispersive spectrometry (SEM/EDS) uses an electron beam generated in a vacuum chamber to image the sample. Samples are prepared by extracting volatile hydrocarbons and drying at low temperature. The cleaned and dried samples are subsequently sputter-coated with a 30 Angstrom thick layer of gold under vacuum. As the electron beam strikes the sample surface, topography sensitive secondary electrons are generated, collected in a detector, and computer imaged. X-rays are also generated while the sample is being scanned. The energy levels of these X-rays are characteristic of the elements from which they were generated. The X-ray energies are computer-imaged into an elemental (EDS) spectrum showing qualitative atomic composition of the sample. SEM/EDS techniques are used to provide both high and low magnification views of the sample with great depth of field, yielding interpretations of the interrelationships between grains, pore types, cements, and clays. SEM techniques are particularly useful in assessing the occurrence of clays within the pore network.

X-Ray Powder Diffraction

X-ray powder diffraction (XRD) is an analytical technique that bombards a finely-powdered rock sample with monochromatic Cu Kα radiation and measures intensity of the scattered beam versus 2-theta angle of the instrument. Minerals are identified by comparing calculated d-spacings with a library of standard d-spacings. *Bulk XRD samples* are prepared by mechanically grinding the sample to a fine powder (< 5 μm) and back-packing the powder into a hollow-cavity sample mount. *Clay samples* are prepared by separating the clay size-fraction from a bulk sample, and depositing a slurry containing the "clays" onto a glass slide. Additional treatments of clay samples by glycolating (to distinguish expandable mixed-layer clays) and heat treating (to discern kaolinite from chlorite) are performed as needed. Quantitative XRD analysis is effected using a whole-pattern fitting method utilizing measured and calculated XRD scans. The XRD measurements are commonly combined with a chemical analysis of the bulk sample (from X-ray fluorescence measurements) to improve the quantitative results. X-ray diffraction analysis provides data on the relative abundances of bulk and clay minerals present in rock samples analyzed, which are often critical to stimulation treatment design.

Permeability/Porosity Sample Preparation

Coreplugs are drilled from wholecore segments using 1” or 1.5” diameter core bits, utilizing a refined mineral oil for lubrication and cuttings removal. The coreplugs are trimmed to right cylinders using a trim saw equipped with a diamond blade. Hydrocarbon solvents refluxing in heated soxhlets are used to extract residual hydrocarbons, and methanol is similarly used to remove pore or coring-filtrate salts. As a function of the lithology, the coreplugs are dried in either a convection or humidity oven to stable weights, and cooled prior to further analysis. Poorly-cemented samples are drilled with liquid nitrogen to stabilize the core, and mounted in nickel sleeves using screens to prevent grain loss.

Porosity and Gas Permeability

Helium porosities (ϕ): The Ultra-Pore 300 is a computerized Boyle's Law porosimeter used to determine the porosity of porous media. The technique uses a combination of the sample's grain volume and bulk volume to calculate porosity. Cleaned and dried core plugs of known weight and dimensions (bulk volume) are placed in a calibrated matrix cup. The grain volume is determined from the expansion of a known mass of helium into a calibrated sample holder.

The porosity fraction is calculated from the relationship between the grain volume and the bulk volume (dimensions). Grain density and pore volume are calculated from the measured weight, bulk volume and grain volume.

Gas permeability (K_g) measured at ambient conditions is a specific permeability to gas (100% gas saturation). Cleaned and dried coreplugs are placed in a Hassler-type core holder and confining stress is applied to prevent gas bypass during permeability testing. Nitrogen gas is flowed through the plug until constant upstream and downstream pressures, and constant flow rate are obtained. Darcy's equation for laminar gas flow is used to calculate specific gas permeability.

The Pulse Decay Permeameter (PDP-200) is a computerized permeameter that is utilized to measure ultra-low permeability in exceptionally tight rock. The system measures permeability ranging from 1 millidarcy to 10 nanodarcies using Helium gas. Core samples are loaded into a hydrostatic core holder and confining pressure is applied. The sample is saturated with gas to pre-equilibrium. Depending on the nature of the rock, saturation can take minutes or hours. The PDP-200 operates using differential pressure transducers that measure a pressure pulse initiated through the rock. Absolute Pressure, Differential Pressure and Time are computer-monitored as the pulse approaches equilibrium. Unsteady state measurements are taken at as the sample approaches pressure equilibrium. Permeability is calculated from the combination of the differential form of Darcy's Equation and the continuity equation.

Capillary Suction Time Testing

The CST test is a fundamental filtration method for determining the electrolyte concentration that will produce the maximum inhibiting effect on a formation. Disaggregated sub-samples of formation material are sieved through a 30 U.S. Mesh screen and mixed at a liquid/solid ratio of 20:1 for several minutes in selected fluids. A small amount of this fluid/rock slurry is placed in a cylinder which is resting upon a standard porous paper. Electrodes are located 0.5 and 1.0 cm from the edge of the cylinder and connected to a timer which measures the time required for the filtrate to travel from the electrode closest to the cylinder to the farthest electrode. The time interval measured depends on the amount of free water in the rock/fluid slurry and the permeability of the filter cake deposited. When comparing the same sample in different fluids, the longer CST times indicate poorer clay control by the fluid. CST data is also presented for comparative purposes as a ratio: fluid with sample divided by the fluid to yield a normalized CST response.

Technology Center Report No.	T-14-12-1209
Reported by:	Michael Wilson & BJ Davis
Requested by:	Edwin Post
Location:	Kenai, Alaska
Analyzed by:	Michael Wilson, Amber Koch, Dr. Gerald Braun, BJ Davis
Distribution:	Edwin Post, Kenneth Nix, Joshua Herald, David Susko, PPTC File

The above data is supplied solely for informational purposes, and Baker Hughes makes no guarantees or warranties, either expressed or implied, with respect to the accuracy or use of these data and interpretations. All product warranties and guarantee shall be governed by the standard contract terms at the time of sale.